

# Optimization of spatial and temporal discretization schemes for Computational Aero Acoustics problems

L. Rández

Departamento de Matemática Aplicada - IUMA

Universidad de Zaragoza. c/ Pedro Cerbuna 12, 50009 Zaragoza, SPAIN.

*Premio a la Investigación de la Academia 2012. Sección de Exactas*

## Abstract

In this paper new finite difference (FD) and Runge–Kutta schemes for Computational Aero Acoustics (CAA) that minimize the total dispersion and dissipation errors arising in the spatial and temporal discretization process are derived. The available parameters in the spatial discretization as well as in the time marching Runge–Kutta scheme are selected so that they minimize a measure of the total dispersion and dissipation errors for linear wave propagations. These schemes are fourth-order accurate in space with finite differences and a resolution with number of points greater or equal to nine together with fourth-order six-stage low storage Runge–Kutta methods for the time integration. The new schemes are tested on a one dimensional convection equation involving long-range sound propagation, and on one-dimensional Euler problems. The numerical results obtained with these test problems indicate an important improvement in accuracy and in numerical efficiency when they are compared with other low dispersive and low dissipative explicit schemes recently published.

**Key Words:** Computational Aero Acoustics; Low dispersion and dissipation; Finite difference schemes; Low storage Runge–Kutta methods; Optimization

**AMS classification:** 65C20; 65M20; 76Q05

## 1 Introduction

In the field of Computational Aero-Acoustics (CAA) the prediction of sound far from its source implies the need of accurate and stable numerical algorithms. As it has been widely recognized [3, 19, 21] stable and high order convergent schemes do not guarantee

a good behavior in the numerical approximation of aero acoustics problems. The main reason is that acoustic waves are non-dispersive and non-dissipative in their propagation and can travel long distances in all directions. Consequently, the numerical schemes must be designed by minimizing the dispersion and dissipation errors in long-time integrations. Note that in standard computational fluid dynamics (CFD) codes a dissipation (in many cases artificial) is included to stabilize the schemes and therefore such schemes are not suitable for CAA problems. In addition, to minimize the dispersion and dissipation errors for the required range of frequencies, large stability limits of the time advancing scheme are also necessary to control the error propagation and also low storage algorithms to improve the efficiency of high dimensional problems must be taken into account.

The construction of optimized time advancing Runge–Kutta (RK) schemes have been considered by several authors [1, 4, 5, 6, 10, 12, 13, 20] which propose a number of low dispersive and low dissipative RK algorithms in standard or in low storage form.

Concerning the spatial discretization, standard schemes have at least second or fourth-order of accuracy and for symmetric stencils they pay special attention to dispersion error. So, in a number of papers [10, 16, 17, 18, 22] Pade or compact type, finite volume (FV) and finite difference (FD) schemes have been proposed by choosing the available parameters so that they minimize the dispersion error. Recently, Bogey and Bailly [3] have optimized central FD schemes with a number of points greater or equal to nine for spatial derivation by minimizing their dispersion and dissipation errors in a range of wavenumbers. Such optimal schemes have algebraic order four and permit calculate linear waves with about four points per wavelength for an accuracy limit, and they are shown to be more accurate and efficient than the standard FD schemes of high order. These authors also have optimized RK algorithms with five and six-stages for time advancing by minimizing their dispersion and dissipation errors for the same range of wavenumbers. These optimized RK algorithms have algebraic order two, and they are shown to be more efficient than the standard fourth-order RK method. Next, Berland *et al.* [2] have optimized a fourth-order six-stage low storage RK algorithm that has similar properties to RK algorithms given in [3] for linear operators, and in addition it is more adequate for nonlinear problems because of its high algebraic order.

All optimal time advancing RK schemes given in [2, 3, 4, 5, 12] have in common that they are derived by minimizing some measures of the dispersion and dissipation errors introduced by the temporal discretization with some additional stability bounds. Clearly these schemes make sense when applied to very accurate space discretizations. However, the dispersive and dissipative behavior of a discretization scheme depends on the total dispersion and dissipation errors introduced by the spatial and temporal discretizations. This fact led to Ramboer *et al.* [19] to consider the errors of both discretizations and to

derive some six-stage RK time advancing schemes by selecting the free parameters of the time advancing scheme such that minimize the total dispersion and dissipation errors for two specific spatial discretizations: fourth-order FV (finite volume) compact central and third-order FV upwind discretizations.

In this paper, new six-stage RK time advancing schemes coupled with new symmetric FD spatial discretizations are derived taking into account the total dispersion and dissipation errors introduced by both discretizations. Hence, the spatial and temporal discretizations are optimized simultaneously in contrast with the optimization carried out by other authors [2, 3, 12]. The main difference with the optimization carried out in [19] is that we select also the free parameters of the spatial discretization so that they minimize the total dispersion and dissipation errors. The motivation is to provide explicit numerical schemes according to accuracy and stability requirements usually demanded in CAA. The paper is organized as follows: In section 2 we analyze the dispersion and dissipation errors for schemes constituted by finite differences for the spatial derivation and Runge–Kutta algorithms for the time integration (FD-RK schemes). In section 3 we present the optimization process and we derive optimized FD-RK schemes by minimizing their total dispersion and dissipation errors. These schemes are fourth-order central FD with a number of points greater or equal to nine and fourth-order six-stage RK algorithms. In section 4 we construct the fourth-order six-stage RK algorithms in low storage form. In section 5 some numerical experiments are presented comparing the accuracy and the efficiency of the new optimized FD-RK schemes with other low dispersive and low dissipative explicit schemes given in [2] and [3]. The final section is devoted to conclusions.

## 2 Dispersion and dissipation for FD-RK schemes

In this section we review briefly some results on the Fourier analysis of FD-RK schemes when applied to the linear scalar wave test equation for  $u = u(t, x)$

$$\frac{\partial u}{\partial t} + c \frac{\partial u}{\partial x} = 0, \quad x \in \mathbf{R}, \quad t \geq 0, \quad (1)$$

with a given initial condition  $u(0, x) = \Phi(x)$  where  $c > 0$  is the velocity of the wave.

For the spatial discretization we will consider central finite difference schemes  $\delta_x$  with a  $(2N + 1)$ -point stencil of type

$$\delta_x u(t, x_\ell) = \frac{1}{\Delta x} \sum_{j=-N}^N a_j u_{\ell+j}, \quad u_k = u(t, x_k), \quad (2)$$

where  $\Delta x$  is the mesh spacing and  $x_j = j \Delta x$ . Usually, the real coefficients  $a_j$  are taken such that the approximation (2) is of order  $p$ , i. e.

$$\partial_x u(t, x_\ell) - \delta_x u(t, x_\ell) = \mathcal{O}(\Delta x^p), \quad p \geq 1, \quad (3)$$

and therefore the coefficients  $a_j$  must satisfy the following linear conditions:

$$\sum_{j=-N}^N j^s a_j = \delta_{1,s}, \quad s = 0, 1, \dots, p, \quad (4)$$

where  $\delta_{p,q}$  is the Kronecker delta defined by  $\delta_{1,s} = 0$ ,  $s \neq 1$  and 1 otherwise. It can be easily seen that the maximum attainable order by a symmetric  $(2N + 1)$ -point stencil FD is  $(N + 1)$  for  $N$  even and  $N$  otherwise.

By using the spatial discretization (2), the semidiscretization of the convective equation (1) is

$$\partial_t u_j + \frac{c}{\Delta x} \sum_{\ell=-N}^N a_\ell u_{j+\ell} = 0, \quad j = 0, \pm 1, \dots \quad (5)$$

First, we present the results of some numerical experiments. So, we display in Figure 1 the numerical solution obtained by solving exactly the semidiscretization of the wave equation (1) given by

$$\begin{cases} \partial_t u_j + c \delta_x u_j = 0, & t \in [0, 400], \\ u_j(0) = \Phi(x_j), \end{cases} \quad (6)$$

for the maximum order  $(2N + 1)$ -point symmetric schemes (2) for  $N = 3, 4, 5$  with  $c = 1$ , and the Gaussian initial condition  $\Phi(x) = \Phi_1(x) = 0.5 \exp(-x^2/9)$ ,  $\Delta x = 1$ ,  $x_j = j$ ,  $j = -50, \dots, 450$  at the time instant  $t = 400$  together with the exact solution of the wave equation. Note that the exact solution is a Gaussian type wave that moves from left to right with constant velocity  $c = 1$  preserving its shape, so that  $u(x, t) = \Phi_1(x - t)$ .

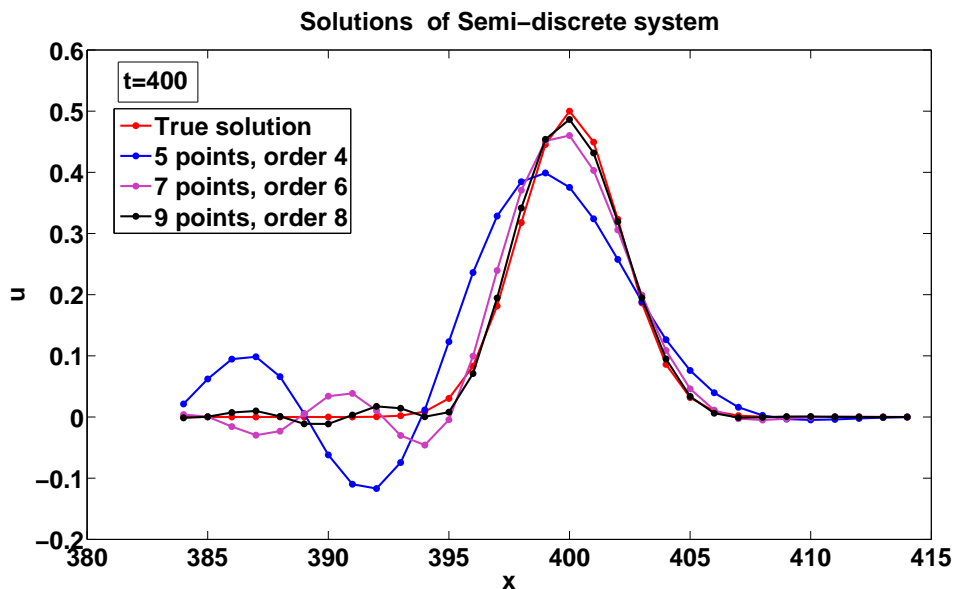


Figure 1: Numerical solution of the linear wave test equation semidiscretized with  $(2N + 1)$ -point central symmetric schemes for  $N = 2, 3, 4$ .

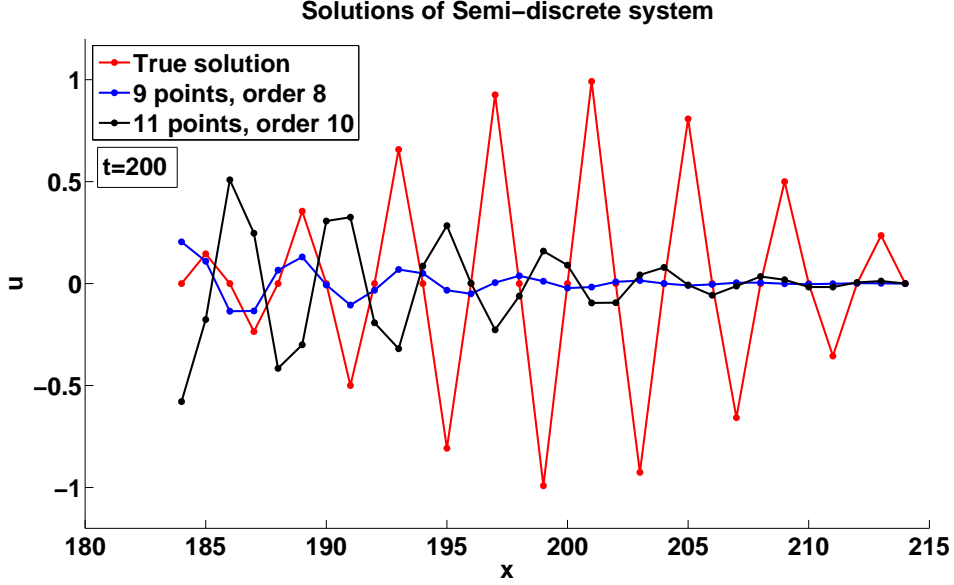


Figure 2: Numerical solution of the wave test equation, Sine-Gaussian initial condition, semidiscretized with  $(2N + 1)$ -point schemes for  $N = 4, 5$ .

From Figure 1, it follows that for in the case of the fourth-order discretization, the spatial dispersion errors introduce strong changes in the shape of the wave and that these changes are smaller when the order increases, but in any case they are not negligible.

In Figure 2 we present the solutions obtained taking a Sine-Gaussian initial condition given by  $\Phi(x) = \Phi_2(x) = \sin(\pi x/2) \exp(-x^2/9)$  for  $\Delta x = 1$ ,  $x_j = -50, \dots, 250$ , where the time interval is  $[0, 200]$ . Now, since the problem is more difficult due to the spectral contents of  $\Phi_2(x)$ , we have taken the higher order spatial symmetric discretizations of orders 8 and 10 corresponding to 9 and 11 points respectively. Now even with the high order spatial discretizations the profile of the wave is destroyed.

In order to explain the behavior of the spatial difference schemes, we apply to (1) and (5) the spatial Fourier transforms given in the continuous and discrete case respectively by

$$\widehat{u}(k, t) = \int_{-\infty}^{\infty} e^{-ikx} u(x, t) dx, \quad \widehat{u}(k, t) = \Delta x \sum_{j=-\infty}^{j=+\infty} e^{-ikx_j} u(x_j, t),$$

obtaining

$$\begin{aligned} \partial_t \bar{u}(k, t) + ick \bar{u}(k, t) &= 0, & \partial_t \widehat{u}(k, t) + ick^* \widehat{u}(k, t) &= 0, \\ k &\in \mathbb{R}, & k &\in [-\pi/\Delta x, \pi/\Delta x], \end{aligned}$$

where  $k^*$  represents the numerical (complex) wavenumber of the FD scheme (i.e., an approximation to the the exact wavenumber  $k$ ) which is given by

$$k^* = -\frac{i}{\Delta x} \sum_{\ell=-N}^N a_\ell e^{i(\ell k \Delta x)}. \quad (7)$$

For a given  $N$ , the quantity  $k^* \Delta x$  is usually called the effective or numerical wavenumber and as follows from (7) is a function of the exact wavenumber  $k \Delta x$ . Further, for a discretization with order  $p$ , exact and effective wavenumbers agree up to order  $(\Delta x)^{p+1}$  and  $(k^* \Delta x)/(k \Delta x) \rightarrow 1$  as  $\Delta x \rightarrow 0^+$ . However when  $k \Delta x \leq \pi$  separates from 0, the dispersion error may become very large. In Figure 3 we show the behavior of  $(k^* \Delta x)$  as a function of  $(k \Delta x)$  for  $2N + 1 = 5, 7, 9, 11$  when  $k \Delta x \in [0, \pi]$ . In all cases  $(k^* \Delta x)$  has a unique maximum  $k_{\max} \Delta x$  in this interval and this implies that clearly those waves with  $k \geq k_{\max}$  will be badly represented by the spatial discretization. In other words, for the  $(2N + 1)$ -point stencil finite difference scheme of maximum order, the spectral components of the initial condition  $\Phi(x)$  with wavenumbers  $k \geq k_{\max}$  are not suitably represented by the discretization (2).

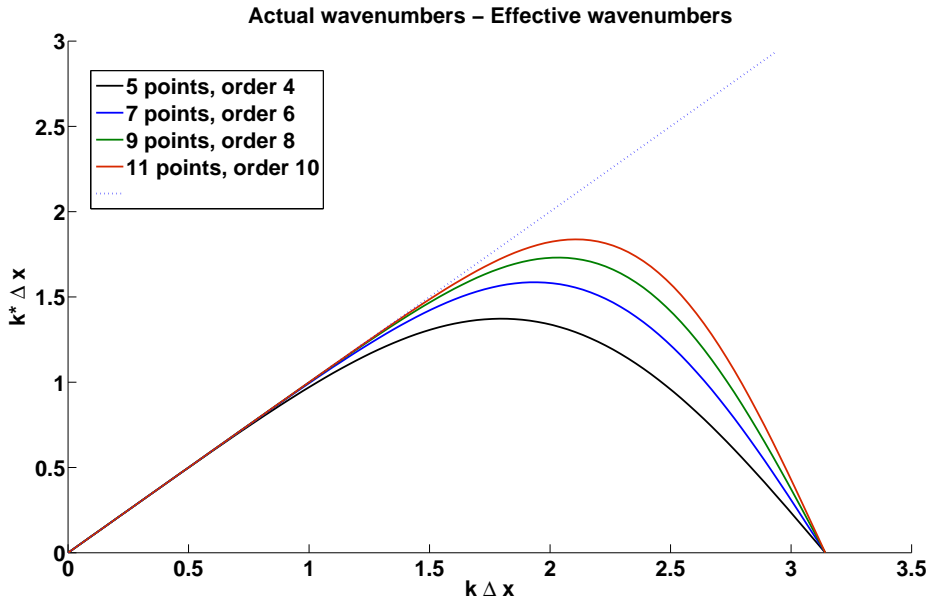


Figure 3: Numerical scaled wavenumbers versus actual scaled wavenumbers.

In addition to this, it has been remarked by several authors [22] that the requirement  $k \leq k_{\max}$  is not enough to ensure a good dispersion behavior of the spatial discretization because even for  $k \lesssim k_{\max}$  the error in the numerical wavenumber can be large. Then, Tam *et al.* [22] introduced the additional condition

$$k \leq k_c = \max \{k \geq 0, |k - k^*| \leq \varepsilon\}, \quad (8)$$

where  $\varepsilon$  is a small quantity that in some practical calculations has been taken empirically as  $\varepsilon = 10^{-3}$  because it leads to a reasonable dispersion error. In Table 1 we present the values of  $k_{\max}$  and  $k_c$  for the high order symmetric FD  $(2N + 1)$ -points schemes with  $N = 2, 3, 4, 5$ .

Table 1: Dispersion values,  $k_{\max}$  and  $k_c$ , for  $(2N + 1)$ -points schemes with  $N = 2, 3, 4, 5$

$2N + 1$	order	$k_{\max}$	$k_c$
5	4	1.37	0.69
7	6	1.59	0.97
9	8	1.73	1.16
11	10	1.84	1.32

Taking into account the values in Table 1 it is possible to explain the numerical results of the above examples. In the first example, since the spectral contents of  $\Phi_1(x)$  is the right half of a Gaussian type function centered at  $k = 0$ , the methods with 11 points are able to deal accurately most of the relevant spectral contents of  $\Phi_1(x)$  (see Figure 4). Nevertheless in the second example, since the Fourier contents is a Gaussian type function centered around  $\pi/2$  all the considered methods cannot include the relevant spectral contents of  $\Phi_2(x)$  and then it is not a suitable discretization for this function. To cope with problems

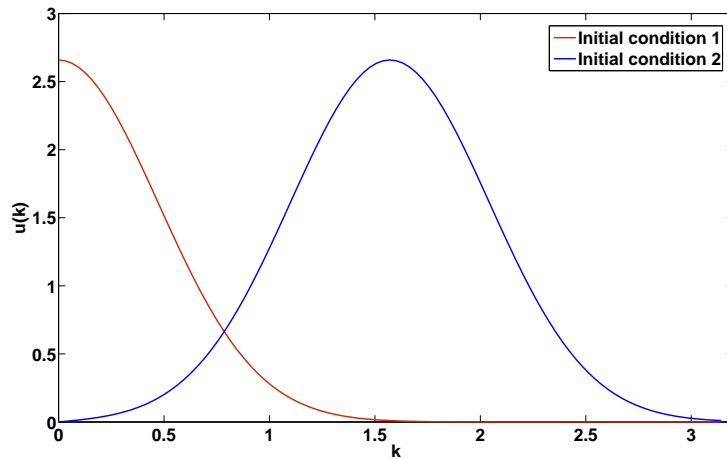


Figure 4: Spectral contents of  $\Phi_i(x)$ .

where the spectral contents of the solution is not close to the origin, several authors have proposed discretizations (2) with order smaller than the maximum order attainable and using the available parameters to get larger values of  $k_{\max}$  and  $k_c$ . This idea was used by Tam and Webb [22] to derive two 7- and 9-point stencil discretizations called DRP (dispersion relation preserving methods) and more recently Bogey and Bailly [3] have constructed other 9-, 11- and 13-points discretizations. In Table 2 we collect the dispersion properties of these methods together with the standard symmetric finite difference ones.

Next, Figures 5 and 6 show the profiles of the semidiscrete and exact solutions at the final time in the above two examples for several optimized schemes. It must be noticed

Table 2: Dispersion values,  $k_{\max}$  and  $k_c$ , for some standard and optimized difference schemes.

method	$2N + 1$	order	$k_{\max}$	$k_c$
Symmetric FD	5	4	1.37	0.69
Symmetric FD	7	6	1.59	0.97
Symmetric FD	9	8	1.73	1.16
Symmetric FD	11	10	1.84	1.32
Tam-Webb	7	4	1.73	1.45
Tam-Webb	9	6	1.77	1.28
Bogey-Bailly	9	4	1.10	1.50
Bogey-Bailly	11	4	1.98	1.66
Bogey-Bailly	13	4	2.14	1.92

that in the second example, the 13-point discretization preserves quite accurately the shape of the wave.

### 2.1 Dispersion and dissipation of the spatial FD scheme

Comparing the exact solution of the linear wave equation (1) with the initial condition  $u(x, 0) = e^{ikx}$  given by

$$u_{\text{ex}}(x, t) = e^{ik(x-ct)}, \quad (9)$$

and the corresponding to the semidiscretization (5)

$$u_{\text{sd}}(x_j, t) = e^{i(kx_j - k^*ct)}, \quad j = 0, \pm 1, \dots, \quad (10)$$

the dispersion and dissipation errors introduced by the spatial discretization are

$$\frac{u_{\text{sd}}(x_j, t)}{u_{\text{ex}}(x_j, t)} = e^{i(k-k^*)ct} = \underbrace{e^{\text{Im}(k^*)ct}}_{\text{dissipation}} \underbrace{e^{i(k-\text{Re}(k^*))ct}}_{\text{dispersion}}. \quad (11)$$

If we denote

$$\phi_s(z) := k\Delta x - \text{Re}(k^*\Delta x) = z - \sum_{j=1}^N (a_j - a_{-j}) \sin(jz), \quad (12)$$

$$d_s(z) := \text{Im}(k^*\Delta x) = -a_0 - \sum_{j=1}^N (a_j + a_{-j}) \cos(jz), \quad (13)$$

equation (11) can be expressed as

$$\frac{u_{\text{sd}}(x_j, t)}{u_{\text{ex}}(x_j, t)} = [e^{d_s(z)} e^{i\phi_s(z)}]_{\frac{ct}{\Delta x}}. \quad (14)$$

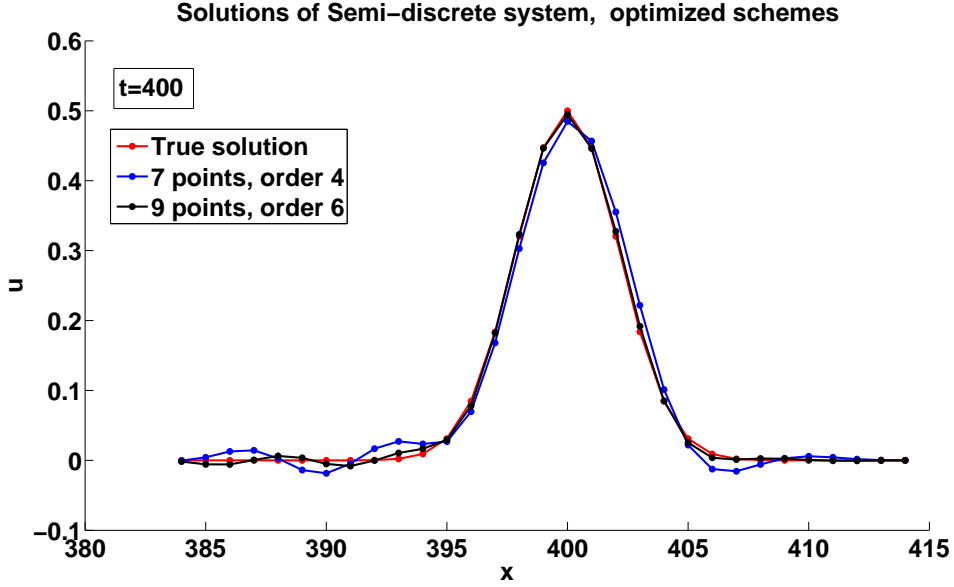


Figure 5: Numerical solution of the wave test equation, Gaussian initial condition, with optimized schemes with  $N = 3, 4$ .

Thus, the spatial dispersion error is:  $\phi_s(z)$ , the spatial dissipation error is:  $1 - e^{d_s(z)}$ , and the central FD scheme is dispersive of order  $q$  and dissipative of order  $r$  if

$$\phi_s(z) = \mathcal{O}(z^{q+1}), \quad d_s(z) = \mathcal{O}(z^{r+1}), \quad z \rightarrow 0. \quad (15)$$

If we consider symmetric FD schemes, then the coefficients satisfy

$$a_0 = 0, \quad a_j = -a_{-j}, \quad j = 1, \dots, N, \quad (16)$$

and in this case it follows from (7) that  $k^*$  is real and the schemes are zero-dissipative, i. e.

$$d_s(z) = 0, \quad \phi_s(z) = z - 2 \sum_{j=1}^N a_j \sin(jz). \quad (17)$$

## 2.2 Dispersion and dissipation of the time advancing RK scheme

To advance the solution  $U(t) = (u_j(t))$  of a general differential system in ODE's

$$\partial_t U = F(t, U), \quad (18)$$

from the time level  $t^n$  to the next time level  $t^{n+1} = t^n + \Delta t$  we will use explicit  $s$ -stage RK schemes [9] defined by the Butcher tableau

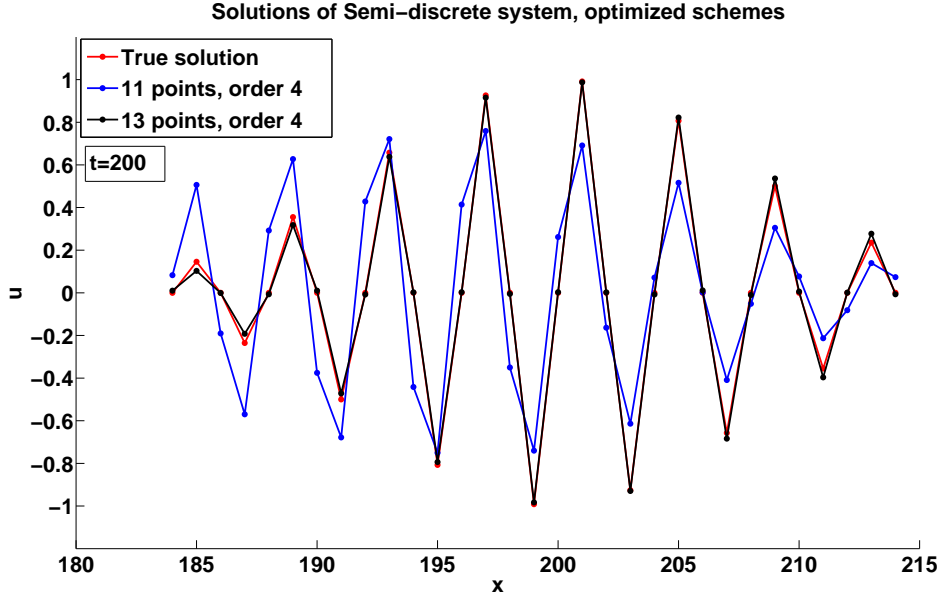


Figure 6: Numerical solution of the wave test equation, Sine-Gaussian initial condition, with optimized schemes with  $N = 5, 6$ .

$$\begin{array}{c|c} \mathbf{c} & \mathbf{A} \\ \hline & \mathbf{b}^T \end{array} = \begin{array}{c|ccc|c} 0 & 0 & & & \\ c_2 & a_{21} & 0 & & \\ \vdots & \vdots & \ddots & \ddots & \\ c_s & a_{s,1} & \cdots & a_{s,s-1} & 0 \\ \hline & b_1 & \cdots & b_{s-1} & b_s \end{array} \quad (19)$$

with  $\mathbf{c} = \mathbf{A}\mathbf{e}$ ,  $\mathbf{e} = (1, \dots, 1)^T$ ,  $\mathbf{b} \in \mathbb{R}^s$ . These coefficients  $b_j, c_j$ , and  $a_{jk}$  are real constants that define the method. The step from  $U^n$  at the time level  $t^n$  to  $U^{n+1}$  at the time level  $t^{n+1}$  can be written as

$$\begin{aligned} U^{n+1} &= U^n + \Delta t \sum_{i=1}^s b_i F_i, \\ F_i &= F(t^n + c_i \Delta t, U^n + \Delta t \sum_{j=1}^{i-1} a_{ij} F_j), \quad i = 1, \dots, s. \end{aligned} \quad (20)$$

For autonomous equations  $F(t, U) = \Lambda U$  with a linear operator  $\Lambda$ , the algorithm (20) becomes

$$U^{n+1} = R(\Delta t \Lambda) U^n, \quad (21)$$

where  $R(\zeta)$  is the so called amplification function of (19) given by

$$R(\zeta) = 1 + \zeta \mathbf{b}^T (\mathbf{I} - \zeta \mathbf{A})^{-1} \mathbf{e}, \quad \zeta \in \mathbb{C}. \quad (22)$$

For explicit  $s$ -stage RK schemes the amplification function is a polynomial of degree  $\leq s$  given by

$$R(\zeta) = 1 + \sum_{\ell=1}^s \gamma_{\ell} \zeta^{\ell}, \quad (23)$$

with  $\gamma_{\ell} = \mathbf{b}^T \mathbf{A}^{\ell-1} \mathbf{e}$ , and it satisfies

$$|R(-ix)| = |R(ix)|, \quad \arg R(-ix) = -\arg R(ix), \quad \forall x \in \mathbb{R}. \quad (24)$$

Note that if the RK scheme (19) has linear order  $p$  then  $\gamma_{\ell} = 1/\ell!$ ,  $\ell = 1, \dots, p$ , and (23) is an approximation to the exponential function  $e^{\zeta}$  at the origin at least of the same order.

In order to illustrate the behavior of standard RK time integrators, we start considering the application of the classical four-stage fourth-order RK4 method with a fixed step size to the semidiscretization (6) with initial condition  $\Phi(x) = \Phi_1(x)$ . Concerning the choice of the step size recall that when a scalar linear problem  $y' = \lambda y$  is integrated by a one step method, the solution satisfies  $y(t_n + \Delta t) = e^{\lambda \Delta t} y(t_n)$  whereas the numerical solution satisfies  $y_{n+1} = R(\lambda \Delta t) y_n$ , where  $R(z)$  is given by (23). Note that all eigenvalues of the semidiscretization (6) are pure imaginary simple  $\pm iw$  and then to satisfy the stability requirement we should have  $|R(iw \Delta t)| \leq 1$  for all  $w \in [0, ck_{\max}]$ . On the other hand it is well known that the (imaginary) stability interval of the fourth-order RK is  $[-2\sqrt{2}, 2\sqrt{2}]$ , thus if we take the DRP spatial discretization of Tam and Webb [22] with 9-points and order 6, according to Table 2,  $1.77\Delta t \leq 2\sqrt{2}$  which implies  $\Delta t \leq 1.597$ . Figure 7 shows the profiles of the numerical and exact solution with  $\Delta t = 1.597$  at the final time level. This example shows large phase and amplitude errors in the numerical solution. In addition, similar experiments with  $\Delta t = 1$  show smaller but not negligible errors and to get accurate solutions, time steps of  $\Delta t \simeq 0.5$  are necessary. These experiments imply that in the standard RK4 stepsizes much smaller than the stability limit are necessary to preserve the dissipation and dispersion properties of this wave type solutions.

Now observe that as remarked above for all wavenumber  $k$  the discrete function ( $e^{ikx_j}$ ) is an eigenfunction of the linear operator  $\Lambda$  defined by (5) corresponding to the eigenvalue  $-ick^*$ . Hence the Fourier wave  $u_j(t) = \beta_k(t) e^{ikx_j}$ ,  $j = 0, \pm 1, \dots$  will be a solution of (5) iff

$$\partial_t \beta_k(t) = -ick^* \beta_k(t), \quad (25)$$

and the exact solution of (5) with  $U^n = (e^{ikx_j})$  is

$$U_{\text{ex}}^{n+1} = e^{-ick^* \Delta t} U^n. \quad (26)$$

By linearity, the corresponding solution (numerical solution) of the RK scheme will be

$$U_{\text{RK}}^{n+1} = R(-ick^* \Delta t) U^n. \quad (27)$$

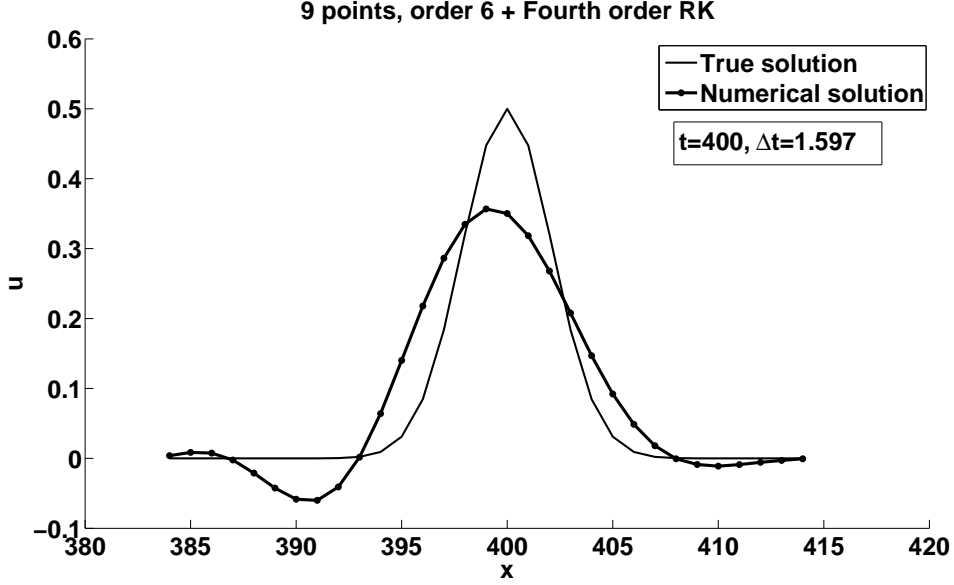


Figure 7: Numerical solution of the wave test equation, Gaussian initial condition, with DRP sixth-order spatial discretization and classical fourth-order RK for time discretization.

As a consequence of (26) and (27) the dispersion and dissipation errors introduced by the temporal discretization at the wavenumber  $k$  are defined by

$$\frac{U_{\text{RK}}^{n+1}}{U_{\text{ex}}^{n+1}} = \frac{R(-ick^* \Delta t)}{e^{-ick^* \Delta t}} = \underbrace{|R(-i\theta)| e^{-\text{Im}(\theta)}}_{\text{dissipation}} \underbrace{e^{i(\text{Re}(\theta) + \arg R(-i\theta))}}_{\text{dispersion}}, \quad (28)$$

where  $\theta = ck^* \Delta t$ , and they are given, respectively, by

$$\phi_t(\theta) = \text{Re}(\theta) + \arg R(-i\theta), \quad d_t(\theta) = 1 - |R(-i\theta)| e^{-\text{Im}(\theta)}. \quad (29)$$

For the case of symmetric FD schemes,  $\theta$  is real ( $\text{Im}(k^*) = 0$ ) and equations (28)–(29) reduce to

$$\frac{U_{\text{RK}}^{n+1}}{U_{\text{ex}}^{n+1}} = \frac{R(-ick^* \Delta t)}{e^{-ick^* \Delta t}} = \underbrace{|R(i\theta)|}_{\text{dissipation}} \underbrace{e^{i(\theta - \arg R(i\theta))}}_{\text{dispersion}}, \quad (30)$$

$$\phi_t(\theta) = \theta - \arg R(i\theta), \quad d_t(\theta) = 1 - |R(i\theta)|. \quad (31)$$

This analysis has led in the last decade to the construction of special RK time advancing schemes taking into account instead of the usual order-stability properties the following ones:

- C1) Stability:  $|R(iw\Delta t)| \leq 1$  for all  $w \in [0, ck_{\text{max}}]$ .

- C2) Dissipation error:  $|1 - R(iw\Delta t)|$  small for all  $w \in [0, ck_c]$ .
- C3) Dispersion error:  $|\arg R(iw\Delta t) - w\Delta t|$  small for all  $w \in [0, ck_c]$ .
- C4) Maximum linear and non linear order. In the linear case defined by the maximum  $p$  such that  $R(z) - e^z = \mathcal{O}(z^{p+1})$ , and in the non linear case by Butcher's conditions.
- C5) Low storage implementation.

The last requirement C5) has been introduced because in practical calculations (typically 2D and 3D-dimensional problems of CAA) the number of spatial grid points and consequently the dimensionality of the system can be very high.

Therefore, as remarked by several authors (see e.g. [5], [7], [8], [20], [23], [14], [15]), effective integrators for practical problems must use the minimum number of registers.

Advancing a step  $U^n \rightarrow U^{n+1}$  with a  $s$ -stage RK method in a problem of dimension  $m$  requires, in general, the storage of  $s + 1$  vectors of dimension  $m$  and there are problems which arise in the semi discretization of some PDEs in which  $m$  is very large. This fact implies that the efficiency of the Runge–Kutta method depends strongly on the number of registers used in the computation and therefore methods with minimum storage requirements are preferred. Thus, for a given number of stages  $s$ , we want to consider minimum storage methods, i.e. that can be implemented with two  $m$ -registers, having the best stability and accuracy properties.

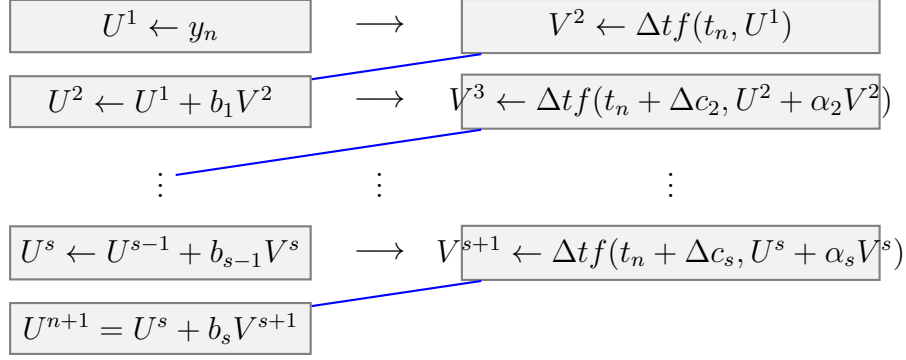
The simplest minimum storage one-step method is Euler's method ( $U^{n+1} = U^n + \Delta t f(t_n, U^n)$ ,  $n = 0, 1, \dots$ ) that requires only two  $m$ -registers and consequently the simplest  $s$ -stage minimum storage method results of a repeated application of Euler's method with step sizes  $c_j \Delta t$ ,  $j = 1, \dots, s$  with  $\sum_{j=1}^s c_j = 1$ , however their accuracy is not enough in many applications. Within the minimum storage schemes (two registers of size  $m$ ), the ( $W$ )-schemes of Williamson [23] have been very popular in Computational Aero Acoustics (CAA) problems in the last years. These ( $W$ )-schemes can be defined by the algorithm:

```

Data:  $V^1 = 0, \quad U^1 = y_n$ 
Result:  $y_{n+1} = U^{s+1}$ 
for  $j = 1$  to  $s$  do
  |  $V^{j+1} = \alpha_j V^j + f(t_n + c_j \Delta t, U^j)$ 
  |  $U^{j+1} = U^j + \Delta t \beta_{j+1} V^{j+1}$ 
end

```

**Algorithm 1:** Williamson scheme



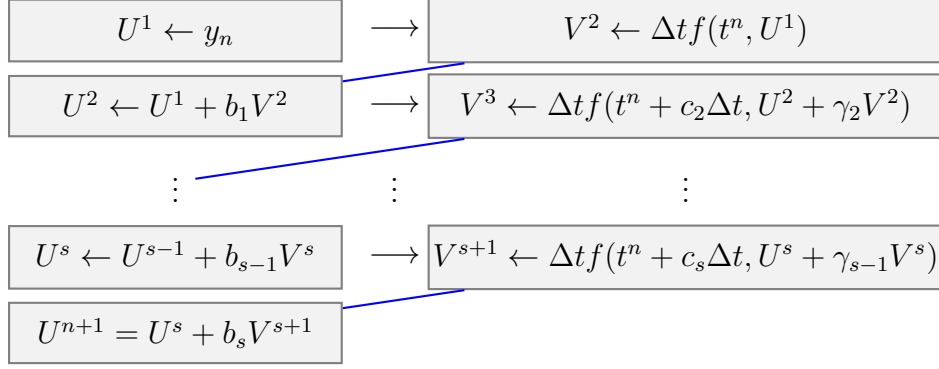
Here,  $\alpha_j, \beta_{j+1}, j = 1, \dots, s$  are the  $2s$  free parameters, but noting that  $V^1 = 0$ , then  $\alpha_1$  is redundant and it is usual to choose  $\alpha_1 = 0$ .

Thus Stanescu and Habashi [20] have derived several ( $W$ )-schemes with amplification functions obtained by Hu *et al.* [12] that minimize the dissipation and dispersion errors for the linear wave test equation (1). Other fourth-order (non linear) ( $W$ )-schemes with minimum local error were derived by Carpenter and Kennedy [8]. More recently, ( $W$ )-storage schemes addressed to problems in the field of CAA have been proposed in [1], [2]. The advantage of Williamson schemes over Euler's compositions is that  $s$ -stage Williamson methods have  $2s - 1$  free parameters and then allow us to obtain better accuracy and stability properties than in  $s$ -stage Euler's compositions.

Alternative families of minimum storage schemes, proposed by van der Houwen ([11], Eq. 2.2.4') and referred to as ( $vdH$ )-schemes, have been considered also to derive different low storage methods. They have been extensively studied by Kennedy, Carpenter and Lewis [13] to obtain optimal schemes of several orders having in mind the semidiscretization of Navier-Stokes equations including also local error control by embedded pairs (of course with additional storage requirements). Also Calvo *et al.* [4], [5] have obtained some optimal ( $vdH$ )-methods for acoustic problems. The next algorithm shows this class of schemes:

**Data:**  $V^1 = 0, \quad U^1 = y_n$   
**Result:**  $y_{n+1} = U^{s+1}$   
**for**  $j = 1$  **to**  $s$  **do**  
    |  $V^{j+1} = f(t_n + c_j \Delta t, U^j + \Delta t \gamma_j V^j)$   
    |  $U^{j+1} = U^j + \Delta t b_j V^{j+1}$   
**end**

**Algorithm 2:** van der Houwen scheme



It must be noticed that the  $s$ -stage ( $vdH$ )-schemes have also  $2s - 1$  free parameters ( $\gamma_1 = 0$ ) and therefore have the same flexibility than the Williamson methods, although it can be seen that the ( $vdH$ )- and ( $W$ )-families do not contain the same RK methods. Recently, by using the Shu-Osher form, two new general families of low storage explicit Runge–Kutta methods have been given by Ketcheson [14], [15], and Calvo *et al.* [7].

Algorithm 2 expressed in Butcher’s notation is defined by the tableau of coefficients (19) with

$$\begin{aligned} a_{j,j-1} &= b_{j-1} + \gamma_{j-1}, \quad j = 2, \dots, s, \\ a_{j\ell} &= b_\ell, \quad j - 1 \leq \ell \leq s - 2. \end{aligned} \tag{32}$$

Since the requirements C1)–C3) depend only on the amplification function  $R(z) = 1 + \sum_{j=1}^s \gamma_j z^j$ , of the considered RK method, many authors have derived “optimal” methods for several values of the number of stages  $s$ . Thus Hu *et al.* [12] obtained optimal methods for  $s = 4, 5, 6$ . Also Bogey and Bailly [3] have derived optimal methods combined with spatial stencils with 9-, 10- and 11-points. In the same line Calvo *et al.* [4], [5] have derived optimal methods for  $s = 5, 6$ .

To measure the quality of a method defined by  $R(z) = 1 + \sum_{j=1}^s \gamma_j z^j$ , it has been usual to compare the following quantities

$$\begin{aligned} S &= \max\{z > 0, |R(iz)| \leq 1\}, \\ L_d &= \max\{z > 0, ||R(iz)| - 1| \leq 10^{-3}\}, \\ L_\varphi &= \max\{z > 0, |\arg(R(iz)) - z| \leq 10^{-3}\}. \end{aligned} \tag{33}$$

In Table 3 the values of these parameters corresponding to several methods are presented.

In Figure 8 we display the profiles of the exact and numerical solutions of example 1 for the six-stages fourth-order RK method of Calvo *et al.* given in [4] at the final time level. As can be seen, the shape of the wave is reproduced properly even with a large time stepsize  $\Delta t = 1.0$

To end this section let us note that in the frame of implicit RK schemes there are methods such as Gauss ones that possess the best properties of stability and dissipation

Table 3: Values of  $S$ ,  $L_d$  and  $L_\varphi$  parameters for several RK methods

method	order	order (lin.)	stages	$S$	$L_d$	$L_\varphi$
Classic	3	3	3	1.73	0.40	0.49
Classic	4	4	4	2.83	0.73	0.68
Hu <i>et al.</i>	2	2	4	2.85	0.85	0.86
Hu <i>et al.</i>	2	2	5	3.54	1.72	1.35
Hu <i>et al.</i>	3	4	6	1.75	1.41	1.27
Calvo <i>et al.</i>	3	3	5	3.48	0.91	1.09
Calvo <i>et al.</i>	4	4	5	3.48	1.25	0.91
Calvo <i>et al.</i>	4	4	6	3.82	2.00	1.14
Allampalli	3	4	7	5.67	1.28	1.07
Gauss	2	2	1	$\infty$	$\infty$	0.23
Gauss	4	4	2	$\infty$	$\infty$	0.95

( $S = L_d = \infty$ ) although they have a non zero dispersion error that depends on  $s$ . For example, the fourth-order Gauss method has  $L_\varphi = 0.95$ .

In Figure 9 we display the profiles of the exact and numerical solutions of example 1 for the two-stage Gauss method with order four at the final time level. Now, if the spatial discretization has good dissipation and dispersion properties, the time integrator reproduces quite accurately the shape of the solution with the step size  $\Delta t = 1$ . However the main drawback of Gauss methods for CAA problems is its implicitness that entails a very high computational cost.

### 2.3 Dispersion and dissipation of the FD-RK scheme

The total dispersion and dissipation errors introduced by the FD-RK scheme are obtained by comparing the numerical solution of the semidiscretization (5) at the time level  $t^{n+1}$  and  $u_j^n = e^{ik(x_j - ct^n)}$

$$u_j^{n+1} = R(-ick^* \Delta t) e^{ik(x_j - ct^n)}, \quad j = 0, \pm 1, \dots, \quad (34)$$

with the exact solution of (1) with  $u(x, 0) = e^{ikx}$

$$u_{\text{ex}}(x_j, t^{n+1}) = e^{-ick\Delta t} e^{ik(x_j - ct^n)}, \quad j = 0, \pm 1, \dots, \quad (35)$$

and writing the total errors as the product of the spatial errors with the temporal errors

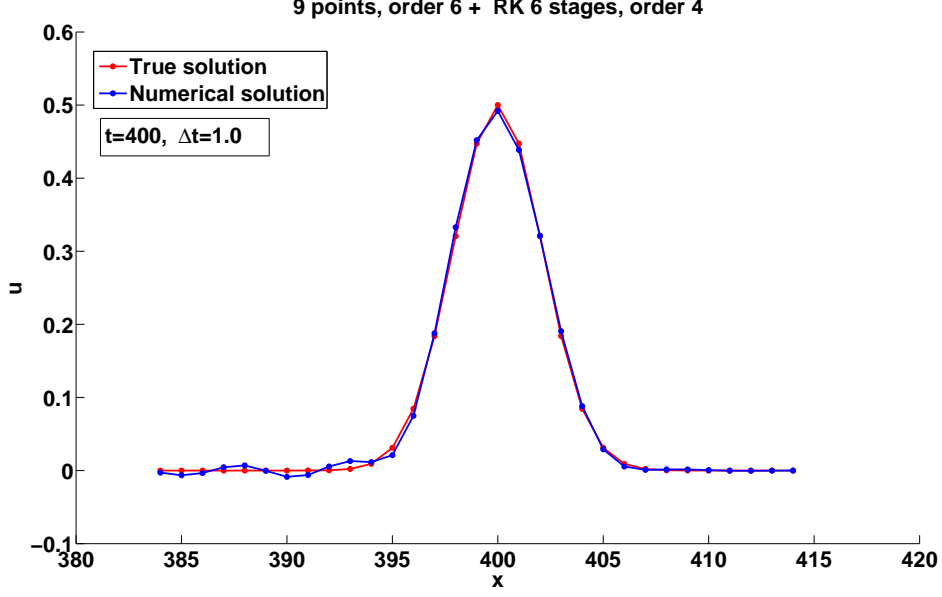


Figure 8: Numerical solution of the wave test equation, Gaussian initial condition, with DRP sixth order spatial discretization and Calvo *et al.* [4] optimized six stages, fourth-order RK for time discretization.

$$\frac{u_j^{n+1}}{u_{\text{ex}}(x_j, t^{n+1})} = \frac{R(-ick^* \Delta t)}{e^{-ick \Delta t}} = \underbrace{\frac{R(-ick^* \Delta t)}{e^{-ick^* \Delta t}}}_{\text{temporal errors}} \underbrace{\frac{e^{-ick^* \Delta t}}{e^{-ick \Delta t}}}_{\text{spatial errors}}. \quad (36)$$

Using the notation:  $\alpha = \frac{c\Delta t}{\Delta x}$  for the CFL number and  $z^* = k^* \Delta x$ , (36) can be written as

$$\frac{u_j^{n+1}}{u_{\text{ex}}(x_j, t^{n+1})} = \underbrace{|R(-i\alpha z^*)|}_{\text{total dissipation}} \underbrace{e^{i[\alpha z + \arg R(-i\alpha z^*)]}}_{\text{total dispersion}}, \quad (37)$$

where

$$z^* = \sum_{j=1}^N (a_j - a_{-j}) \sin(jz) - i \left( a_0 + \sum_{j=1}^N (a_j + a_{-j}) \cos(jz) \right), \quad (38)$$

and the total dispersion and dissipation errors are given, respectively, by

$$\phi_{\text{Tot}}(\alpha, z) = \alpha z + \arg R(-i\alpha z^*), \quad d_{\text{Tot}}(\alpha, z) = 1 - |R(-i\alpha z^*)|. \quad (39)$$

Again, for symmetric FD schemes  $z^* = z - \phi_s(z)$  is real and equations (37) and (39) reduce to

$$\frac{u_j^{n+1}}{u_{\text{ex}}(x_j, t^{n+1})} = \underbrace{|R(i\alpha z^*)|}_{\text{total dissipation}} \underbrace{e^{i[\phi_t(\alpha z^*) + \alpha \phi_s(z)]}}_{\text{total dispersion}}, \quad (40)$$

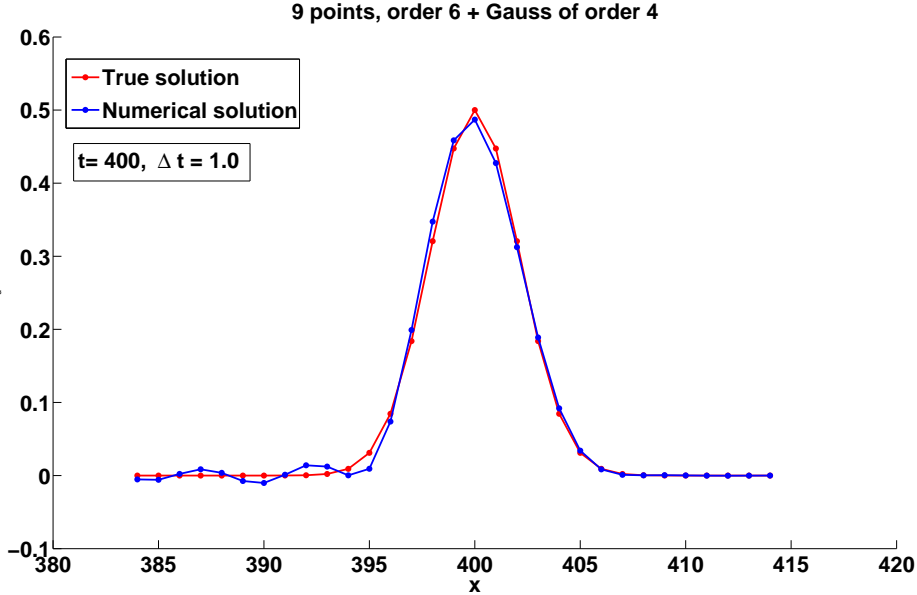


Figure 9: Numerical solution of the wave test equation, Gaussian initial condition, with DRP sixth-order spatial discretization and fourth-order Gauss RK for time discretization.

and we define

$$\phi_{\text{Tot}}(\alpha, z) = \phi_t(\alpha z^*) + \alpha \phi_s(z), \quad d_{\text{Tot}}(\alpha, z) = 1 - |R(i\alpha z^*)|. \quad (41)$$

Next we illustrate the spatial, temporal and total errors for two FD-RK schemes. First of all we combine the standard eighth-order nine-points symmetric FD scheme (SFD9) with the classical four-stage fourth-order RK time advancing algorithm (RK4). In this case there is no dissipation error in the spatial discretization and the total dissipation error is due to the time advancing algorithm. For the dispersion error, we display in Figure 10 the (scaled) spatial, temporal and total errors for  $z = k\Delta x \in [0, \pi/2]$  and  $\alpha = 1$ . It can be seen that for  $z = k\Delta x \leq 0.75$  the effect of the spatial error  $\phi_s(z)$  on the total error  $\phi_{\text{Tot}}(1, z)$  is negligible but for  $z = k\Delta x > 0.75$  the spatial error is comparable or even greater than the temporal error and taking into account that both have the same sign both errors have a cumulative effect on the total error.

As a second scheme we combine the same spatial discretization with the six-stage low-dissipation and low-dispersion RK scheme (RKHu6) given by Hu *et al.* [12]. By the symmetry of the spatial scheme only the temporal dissipation is responsible for the total dissipation error and we focus on the dispersion errors. In Figure 11 we display the spatial, temporal and total errors for  $z = k\Delta x \in [0, \pi/2]$  and  $\alpha = 1$ . In this case a smaller total error  $\phi_{\text{Tot}}$  than in the previous case is obtained but the small temporal error  $\phi_t$  achieved in the optimization of the time advancing scheme RKHu6 is compensated by the large spatial error  $\phi_s$ . However, the computational cost of the scheme RK4 is reduced by a

factor of  $2/3$  with respect to computational cost of the scheme RKHu6. In Figure 12 we show the spatial, temporal and total errors for the scheme SFD9-RK4 at a CFL number  $\alpha = 2/3$  so that both schemes have the same computational cost, and it can be seen that both schemes have a comparable total error  $\phi_{\text{Tot}}$ .

These examples show that in the linear error analysis it is crucial to consider the total errors to achieve optimal schemes.

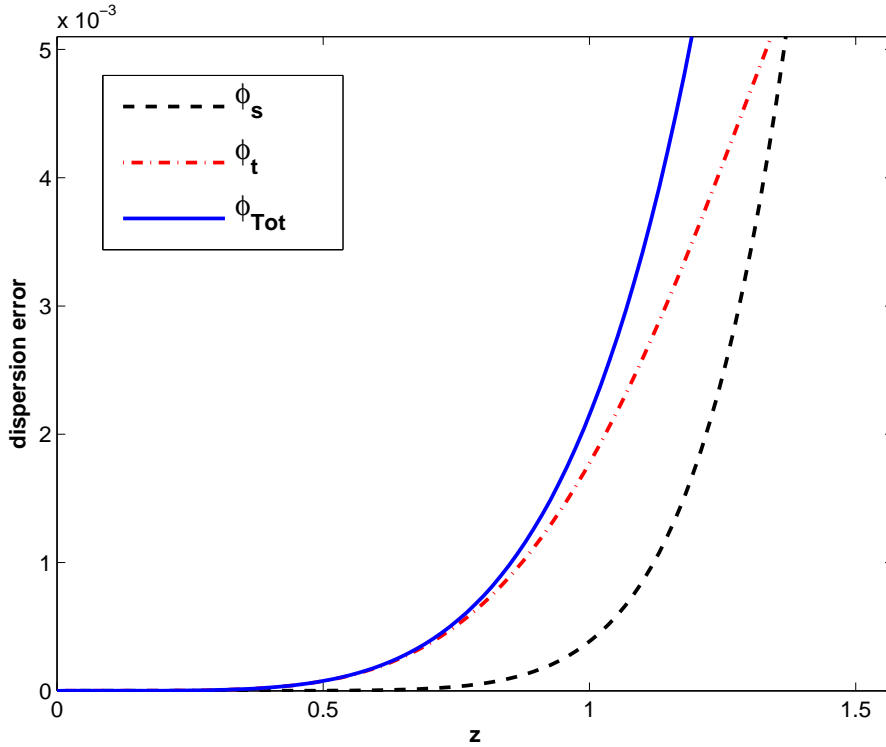


Figure 10: Dispersion errors (scaled by  $1/\pi$ ) for *SFD9-RK4* at  $\alpha = 1$ .

### 3 Optimization of the FD-RK schemes

In this section new FD-RK schemes are derived by minimizing the total dispersion and dissipation errors.

For the spatial discretization we will consider symmetric FD schemes (16) using  $2N+1$  grid points with  $N = 4, 5, 6$ , and accuracy order four. In view of (4), the available coefficients  $a_j$  satisfy the conditions

$$a_0 = 0, \quad \sum_{j=1}^N j a_j = \frac{1}{2}, \quad \sum_{j=1}^N j^3 a_j = 0. \quad (42)$$

and the coefficients  $a_1$  and  $a_2$  can be expressed in terms of  $a_j$ ,  $j = 3, \dots, N$  which will be used as free parameters in the optimization process.

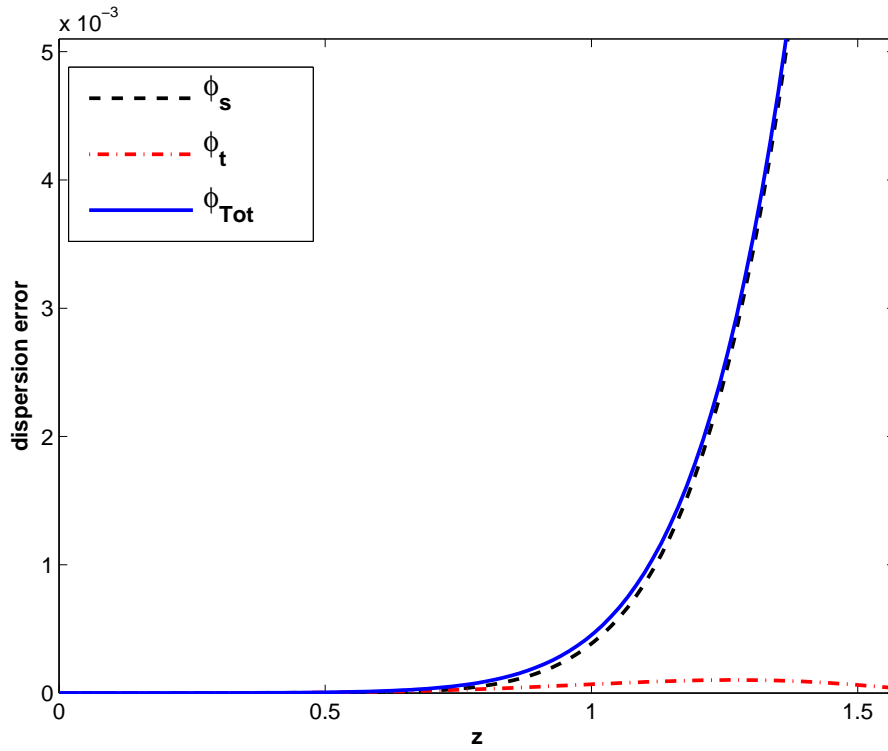


Figure 11: Dispersion errors (scaled by  $1/\pi$ ) for  $SFD9-RKHu6$  at  $\alpha = 1$ .

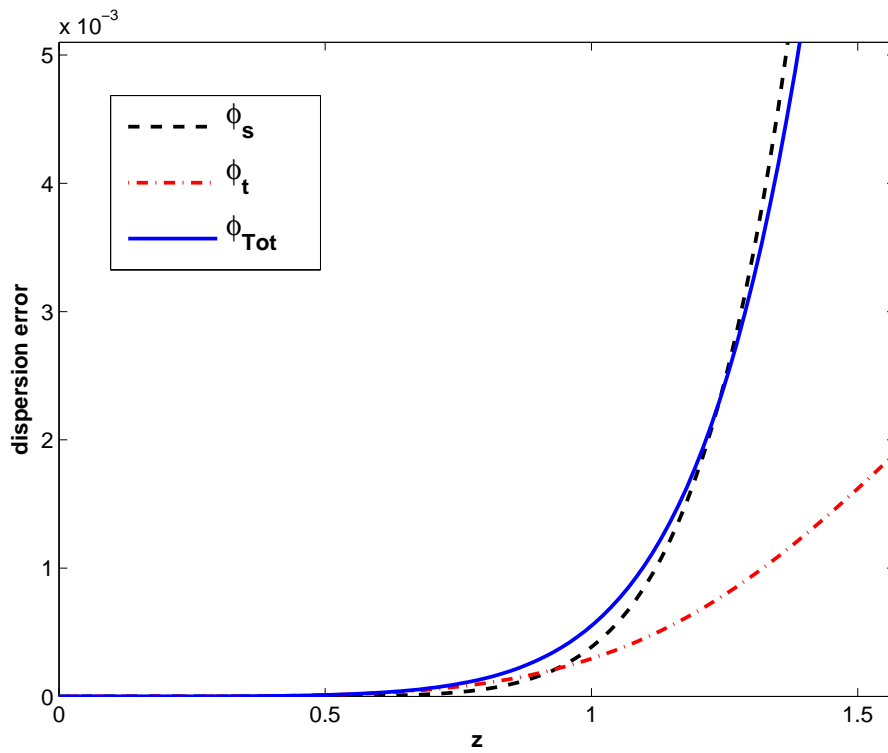


Figure 12: Dispersion errors (scaled by  $1/\pi$ ) for  $SFD9-RK4$  at  $\alpha = 2/3$ .

For time advancing we will use low storage six-stage explicit RK methods with order four. In the application to linear differential equations they are characterized by the amplification function

$$R(\zeta) = 1 + \zeta + \frac{1}{2!} \zeta^2 + \frac{1}{3!} \zeta^3 + \frac{1}{4!} \zeta^4 + \beta_5 \zeta^5 + \beta_6 \zeta^6, \quad (43)$$

with the free parameters  $\beta_5$  and  $\beta_6$ .

Now the resulting schemes, denoted by  $SFD_{2N+1}-RK_6$  with  $N = 4, 5, 6$ , depend on the free parameters  $a_3, \dots, a_N, \beta_5$  and  $\beta_6$  which will be determined by minimizing the following error measure

$$\iint_D \left[ \left( \frac{\phi_{\text{Tot}}(\alpha, z)}{\pi} \right)^2 + d_{\text{Tot}}^2(\alpha, z) \right] d\alpha dz, \quad (44)$$

where the integration region is defined by  $D = \{(\alpha, z) \mid \alpha \in (0, 1], z \in [z_{\min}, z_{\max}]\}$  for some given  $z_{\min}$  and  $z_{\max}$ . Further we impose the stability condition

$$|R(i\alpha z^*)| < 1, \quad \alpha \in (0, 1], \quad z \in (0, z_{\max}], \quad (45)$$

with  $z^*$  given by (38).

We notice that the main difference of (44) with error measures considered by other authors (for example [2, 3, 12, 19]) is the use of the total dispersion and dissipation errors on a two-dimensional region associated to spatial and temporal discretizations. The constraint (45) was imposed in order to obtain optimized schemes which are stable on the range of wavenumbers in which the dispersion and dissipation behavior is acceptable in terms of accuracy.

Here we chose the wavenumbers limits  $z_{\min} = \pi/16$  and  $z_{\max} = \pi/2$  which amounts to consider waves between 32 points per wavelength and 4 points per wavelength, respectively, and for the scheme with  $N = 6$  we also use  $z_{\max} = 3\pi/5$  as in [3]. The coefficients  $\beta_5, \beta_6$  and  $a_j$  obtained for the optimized FD-RK schemes are given in Tables 4 and 5.

To compare the dispersive and dissipative behavior of the new optimized schemes we consider some FD-RK schemes recently published in the scientific literature [2, 3] which have been optimized independently in space and in time. The optimized spatial FD schemes derived in [3] together with the fourth-order six-stage RK algorithm derived in [2], and they will be referred as  $FDo9p-RKB_6$ ,  $FDo11p-RKB_6$  and  $FDo13p-RKB_6$ . Figures 13–18 show the total dispersion and dissipation errors:  $\phi_{\text{Tot}}(\alpha, z)/\pi$  and  $d_{\text{Tot}}(\alpha, z)$  depicted as a function of  $z = k\Delta x$  ( $0 \leq z \leq z_{\max}$ ) at a CFL number  $\alpha = 1$ . These figures show that the new optimized schemes have generally a better dispersive and dissipative behavior than those optimized independently in space and in time, in particular for wavenumbers near to  $z = \pi/2$ .

Next a quantitative comparison of schemes by taking dispersion and dissipation error bounds:  $|\phi_{\text{Tot}}(\alpha, z)/\pi| \leq 10^{-3}$  and  $|d_{\text{Tot}}(\alpha, z)| \leq 10^{-4}$  is given. These limits indicate the maximum wavenumbers  $z = k\Delta x$  properly calculated which can also be expressed in terms of the number of points per wavelength  $N_p = 2\pi/k\Delta x$  with respect to the grid-size  $\Delta x$ . They are reported in Table 6 for the schemes considered in the comparison at a CFL number  $\alpha = 1$ . For the same  $(2N + 1)$ -points stencil, the new optimized schemes have generally better accuracy limits in phase than the schemes optimized independently in space and in time. In addition, waves with four points per wavelength at  $\alpha = 1$  are taken into account only by the schemes  $SFD_{11}\text{-}RK_6(a)$  and  $SFD_{13}\text{-}RK_6(a)$ .

Table 4: Coefficients of the optimized  $SFD_{2N+1}\text{-}RK_6(a)$  schemes with  $z_{\text{max}} = \pi/2$

$N = 4$	$N = 5$	$N = 6$
$\beta_5 = 0.00785313645903$	$\beta_5 = 0.00785780000000$	$\beta_5 = 0.00785812800000$
$\beta_6 = 0.00092656241553$	$\beta_6 = 0.00094507900000$	$\beta_6 = 0.00094851200000$
$a_1 = 0.84332103556666$	$a_1 = 0.88131666666666$	$a_1 = 0.90280686066667$
$a_2 = -0.24646064685333$	$a_2 = -0.29651333333333$	$a_2 = -0.32759725333333$
$a_3 = 0.06024952338000$	$a_3 = 0.09657000000000$	$a_3 = 0.12294034000000$
$a_4 = -0.00778707800000$	$a_4 = -0.02315000000000$	$a_4 = -0.03812260000000$
	$a_5 = 0.00292000000000$	$a_5 = 0.00835681000000$
		$a_6 = -0.00095450400000$

Table 5: Coefficients of the optimized  $SFD_{13}\text{-}RK_6(b)$  scheme with  $z_{\text{max}} = 3\pi/5$

$\beta_5 = 0.00784952503800$
$\beta_6 = 0.00099024688453$
$a_1 = 0.91934276215510$
$a_2 = -0.35241708459276$
$a_3 = 0.14520000000000$
$a_4 = -0.05177590000000$
$a_5 = 0.01379215888197$
$a_6 = -0.00199429789657$

Table 6: Dispersion and dissipation limits in wavenumbers  $z = k\Delta x$  and in points per wavelength  $N_p = 2\pi/k\Delta x$  with respect to the grid-size  $\Delta x$  at  $\alpha = 1$ .

	Dispersion $k\Delta x$	$ \phi_{\text{Tot}}/\pi  \leq 10^{-3}$ $2\pi/k\Delta x$	Dissipation $k\Delta x$	$ d_{\text{Tot}}  \leq 10^{-4}$ $2\pi/k\Delta x$
<i>FD09p-RKB<sub>6</sub></i>	1.43	4.39	1.88	3.34
<i>FD011p-RKB<sub>6</sub></i>	1.44	4.38	1.82	3.45
<i>FD013p-RKB<sub>6</sub></i>	1.40	4.49	1.80	3.49
<i>SFD<sub>9</sub>-RK<sub>6</sub>(a)</i>	1.46	4.31	1.65	3.81
<i>SFD<sub>11</sub>-RK<sub>6</sub>(a)</i>	1.63	3.85	1.74	3.61
<i>SFD<sub>13</sub>-RK<sub>6</sub>(a)</i>	1.74	3.61	1.75	3.56
<i>SFD<sub>13</sub>-RK<sub>6</sub>(b)</i>	1.89	3.32	1.51	4.16

#### 4 Construction of the low storage RK methods

In this section we analyze the low-storage explicit RK methods with  $s = 6$  stages and non linear algebraic order 4 given in the previous section. These schemes satisfy the order conditions

$$\begin{aligned} \mathbf{b}^T \mathbf{e} = 1, \quad \mathbf{b}^T \mathbf{c} = 1/2, \quad \mathbf{b}^T \mathbf{c}^2 = 1/3, \quad \mathbf{b}^T \mathbf{A} \mathbf{c} = 1/6, \\ \mathbf{b}^T \mathbf{c}^3 = 1/4, \quad \mathbf{b}^T (\mathbf{c} \cdot \mathbf{A} \mathbf{c}) = 1/8, \quad \mathbf{b}^T \mathbf{A} \mathbf{c}^2 = 1/12, \quad \mathbf{b}^T \mathbf{A}^2 \mathbf{c} = 1/24. \end{aligned} \quad (46)$$

In addition to the equations given by (46), the coefficients of (32) also satisfy the two additional conditions

$$\mathbf{b}^T \mathbf{A}^3 \mathbf{c} = \beta_5, \quad \mathbf{b}^T \mathbf{A}^4 \mathbf{c} = \beta_6, \quad (47)$$

obtained in the optimization process of the previous section.

Since we have a set of ten nonlinear equations (46)–(47) for the eleven coefficients  $(b_1, \dots, b_6, \gamma_1, \dots, \gamma_5)$ , one parameter is free, and therefore some additional requirements can be imposed for its determination. Here, we use this degree of freedom to solve numerically the nonlinear system (46)–(47) by taking into account standard requirements in the derivation of practical RK methods:

- The weights satisfy  $|b_i| \leq 2$ ,  $i = 1, \dots, 6$ .
- The nodes satisfy  $c_i \neq c_j$ ,  $\forall i \neq j$  and  $0 \leq c_i \leq 1$ ,  $i = 1, \dots, 6$ .
- Minimize the Euclidean norm of the leading term of the local error of the advancing approximation, i.e.  $\|\tau^{(5)}\|_2 = \sum \left| C_j^{(5)} \right|^2$ , where  $C_j^{(5)}$  are the coefficients of the

elementary differentials of order five in the local error expansion in powers of the step size  $\Delta t$ .

We have taken a fine grid in the free parameter and we have tested the first two requirements at each point. From the available points, we have started a minimization process of the third condition and finally the coefficients obtained for the low-storage RK algorithms associated to the optimized schemes of the previous section are given in Tables 7–10.

Table 7: Coefficients of the low-storage RK algorithm for the  $SFD_9$ - $RK_6(a)$  scheme

$c_1 = 0$	$b_1 = 0.11542410418395$	$\gamma_1 = 0.18457589581605$
$c_2 = 0.300000000000000$	$b_2 = 0.14337328928437$	$\gamma_2 = 0.12830567193128$
$c_3 = 0.38710306539960$	$b_3 = 0.34923156739002$	$\gamma_3 = 0.10871574089416$
$c_4 = 0.71674470175250$	$b_4 = -0.52556842961887$	$\gamma_4 = 0.60238704717262$
$c_5 = 0.68484757841209$	$b_5 = 0.49748516677020$	$\gamma_5 = 0.27184007546667$
$c_6 = 0.85178577347634$	$b_6 = 0.42005430199034$	

Table 8: Coefficients of the low-storage RK algorithm for the  $SFD_{11}$ - $RK_6(a)$  scheme

$c_1 = 0$	$b_1 = 0.10974285720869$	$\gamma_1 = 0.18025714279131$
$c_2 = 0.290000000000000$	$b_2 = 0.13448959704914$	$\gamma_2 = 0.13857764418235$
$c_3 = 0.38281009844018$	$b_3 = 0.38294944978031$	$\gamma_3 = 0.08426505141729$
$c_4 = 0.71144695545543$	$b_4 = -0.60216813067103$	$\gamma_4 = 0.66860432485845$
$c_5 = 0.69361809822556$	$b_5 = 0.49945631650501$	$\gamma_5 = 0.30908387736075$
$c_6 = 0.83355396723287$	$b_6 = 0.47552991012788$	

Table 9: Coefficients of the low-storage RK algorithm for the  $SFD_{13}$ - $RK_6(a)$  scheme

$c_1 = 0$	$b_1 = 0.11287033711698$	$\gamma_1 = 0.19025714279131$
$c_2 = 0.300000000000000$	$b_2 = 0.14141097168321$	$\gamma_2 = 0.13989004259688$
$c_3 = 0.38412249685471$	$b_3 = 0.36534072934351$	$\gamma_3 = 0.08964556109275$
$c_4 = 0.71682746513089$	$b_4 = -0.54871438354286$	$\gamma_4 = 0.66668799693474$
$c_5 = 0.69170177030185$	$b_5 = 0.47533937806862$	$\gamma_5 = 0.31691629028663$
$c_6 = 0.84138638015875$	$b_6 = 0.45375296733053$	

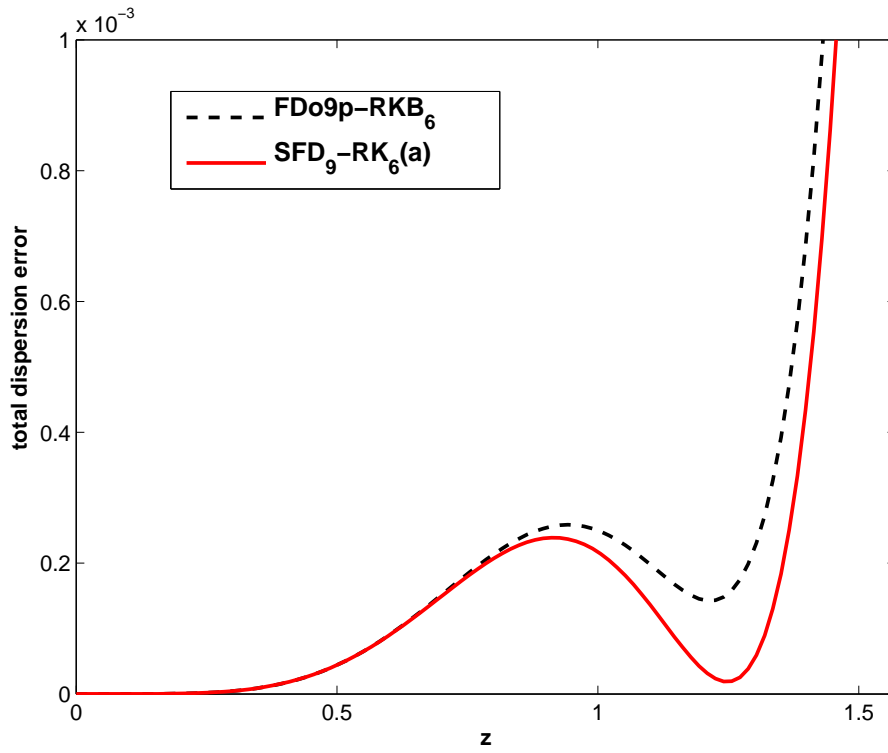


Figure 13: Total dispersion errors at  $\alpha = 1$ .

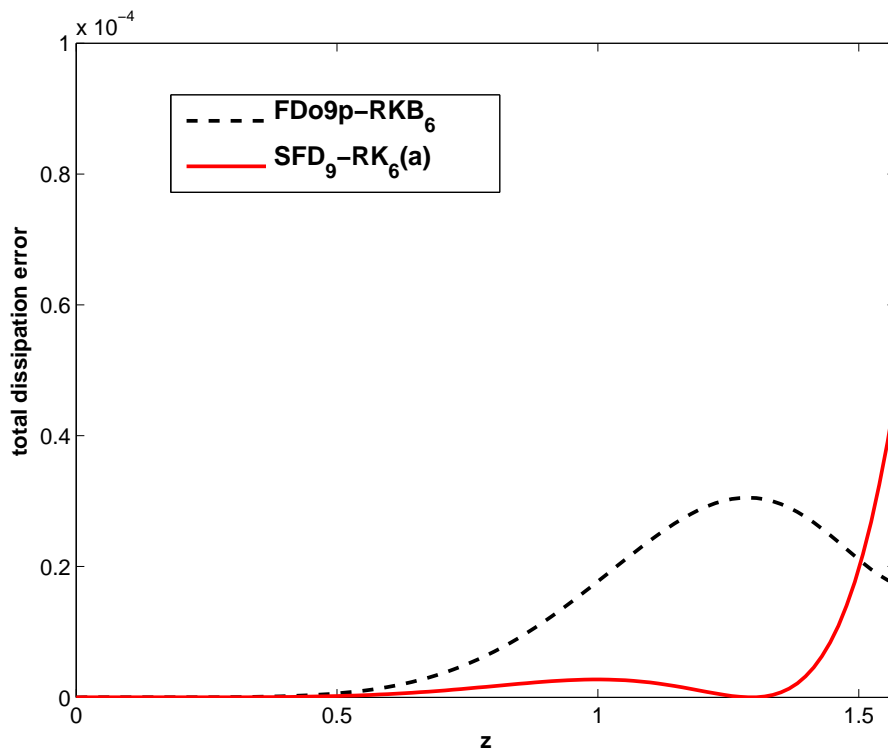


Figure 14: Total dissipation errors at  $\alpha = 1$ .

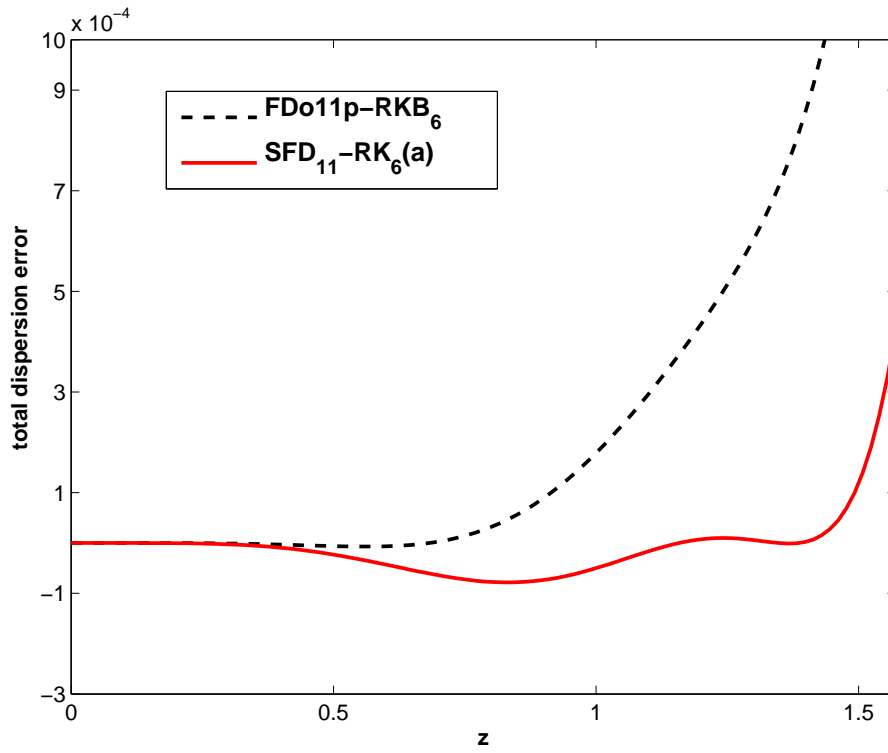


Figure 15: Total dispersion errors at  $\alpha = 1$ .

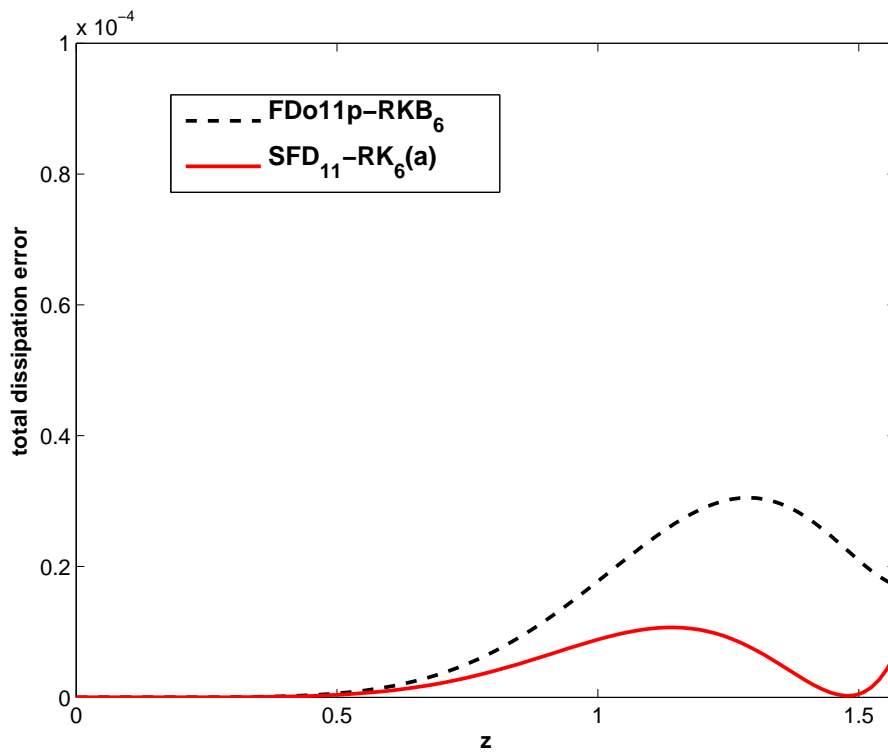


Figure 16: Total dissipation errors at  $\alpha = 1$ .

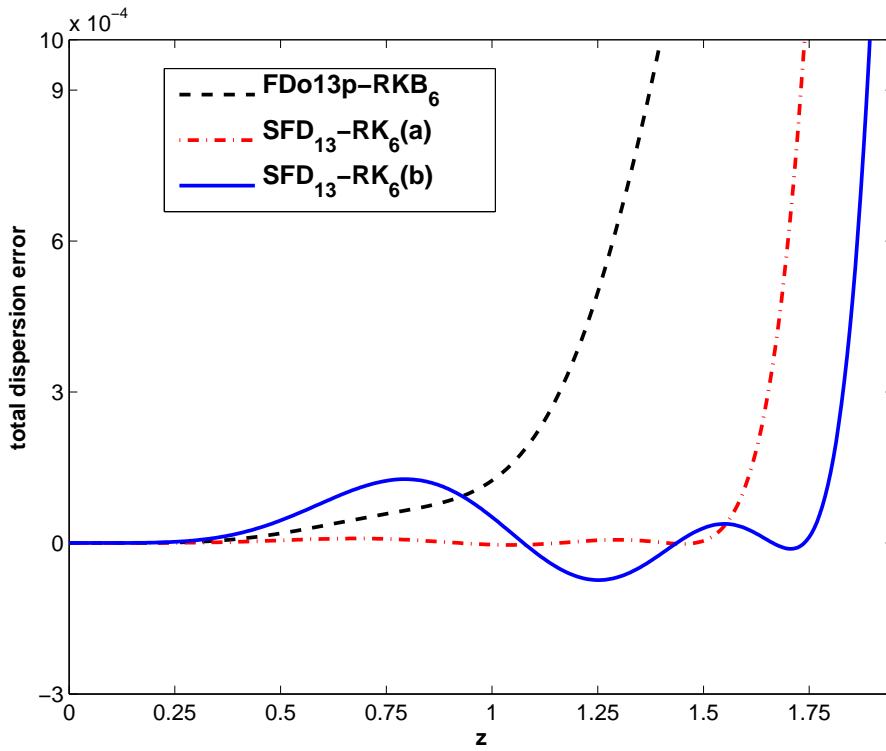


Figure 17: Total dispersion errors at  $\alpha = 1$ .

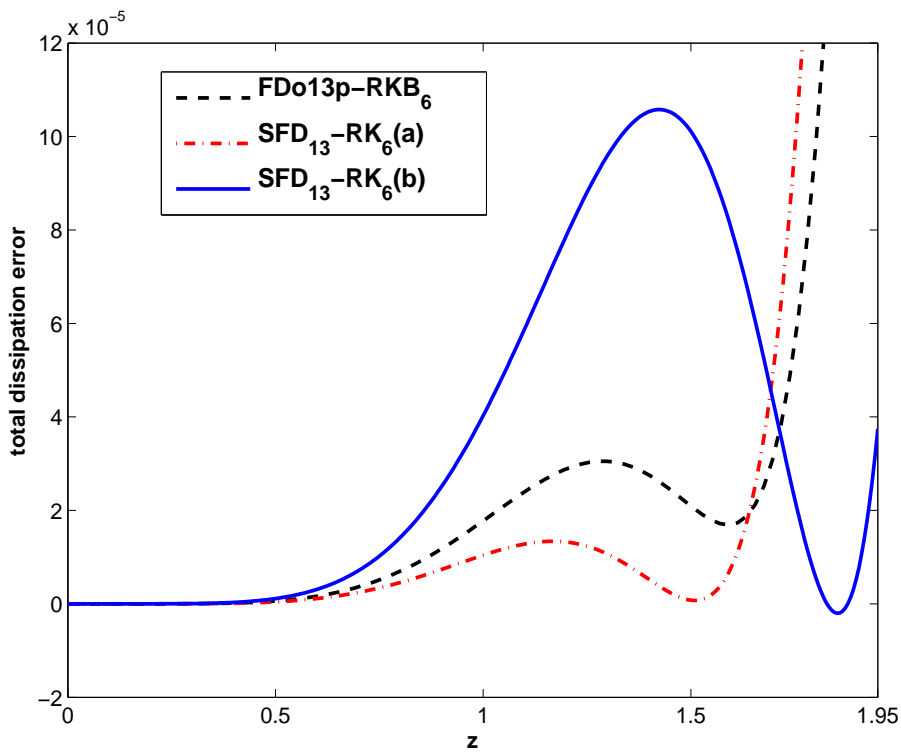


Figure 18: Total dissipation errors at  $\alpha = 1$ .

Table 10: Coefficients of the low-storage RK algorithm for the  $SFD_{13}\text{-}RK_6(b)$  scheme

$c_1 = 0$	$b_1 = 0.11542109063167$	$\gamma_1 = 0.20457890936833$
$c_2 = 0.3200000000000000$	$b_2 = 0.14461329419966$	$\gamma_2 = 0.12109473781601$
$c_3 = 0.38112912264734$	$b_3 = 0.36393100640076$	$\gamma_3 = 0.11419683938110$
$c_4 = 0.73816223061319$	$b_4 = -0.43062100269419$	$\gamma_4 = 0.50989197038198$
$c_5 = 0.70323635891988$	$b_5 = 0.33271255388848$	$\gamma_5 = 0.31562989999482$
$c_6 = 0.84168684242120$	$b_6 = 0.47394305757361$	

## 5 Numerical experiments

In order to test the effectiveness of the optimized low storage RK schemes derived in the above section, we use several model problems with linear and nonlinear wave propagation. In particular, we have considered a one dimensional convection equation involving long-range sound propagation, and two Euler model problems. The new optimized schemes have been compared with the schemes  $FDo9p\text{-}RKB_6$ ,  $FDo11p\text{-}RKB_6$  and  $FDo13p\text{-}RKB_6$  developed in [2, 3].

### 5.1 One dimensional convection equation

In our first numerical experiments we have considered the two basic problems studied by Bogey and Bailly in [3]. The aim is to check the long-range propagation of two initial disturbances by the one-dimensional convective wave equation (1) with  $c = 1$  given by

$$u(x, 0) = \sin\left(\frac{2\pi x}{a\Delta x}\right) \exp\left(-\log(2) \left(\frac{x}{b\Delta x}\right)^2\right),$$

where the parameters  $a$  and  $b$  are  $a = 8$  and  $b = 3$  for the case I and  $a = 4$  and  $b = 9$  for the case II.

As remarked in [3] these choices of  $a$  and  $b$  have been made for the spectral contents of  $u(x, 0)$ . Thus in case I the spectral content of  $u(x, 0)$  is a Gaussian function centered around  $k\Delta x = \pi/4$  with wavenumbers  $k\Delta x \in (0, \pi/2)$  whereas in case II the Gaussian function is centered around  $k\Delta x = \pi/2$ .

For the case I the initial disturbance is propagated over  $800\Delta x$  which corresponds to 100 times the dominant wavelength. Figures 19–24 show the results obtained with the schemes of 9, 11 and 13 points, respectively, for a CFL number  $\alpha = 1$ . Figures 19, 21 and 23 show the solution computed with the numerical schemes whereas Figures 20, 22 and 24 show the total errors given by  $|u_{\text{ex}} - u_{\text{num}}|$ . The solution obtained with the schemes of 9 points (Figure 19) shows dispersion of the initial disturbance for both schemes. In this case the total errors (Figure 20) of the scheme  $FDo9p\text{-}RKB_6$  are slightly smaller than the

total errors of the scheme  $SFD_9-RK_6(a)$ . On the other hand, the results obtained with the 11 and 13-points schemes are different (Figures 21–24). Now the solutions obtained by using the schemes developed in [2, 3] are clearly distorted, whereas the solutions obtained by using the new optimized schemes superpose fairly on the exact solution. It is worth to remark that the total errors presented by the new optimized schemes are at least 2.5 times smaller than the total errors presented by the schemes developed in [2, 3]. These results are in agreement with the better dispersive properties of the new optimized schemes as analyzed in section 3. It should also be noted that the scheme  $SFD_{13}-RK_6(a)$  is more accurate than the scheme  $SFD_{13}-RK_6(b)$  for this problem.

Case II is a test model to investigate if wavenumbers  $z = k\Delta x \simeq \pi/2$  are properly calculated with about four points per wavelength. As remarked in [3] these waves often appear in Large Eddy Simulation (LES) procedures. Now the initial disturbance is propagated over a distance of  $200\Delta x$  which corresponds to 50 times the wavelength. Figures 25–28 show the results obtained with the schemes of 11 and 13 points for a CFL number  $\alpha = 1$ . The schemes of 9 points do not result accurate enough to solve this problem. The Figures 25 and 27 show the solution computed with the numerical schemes and the Figures 26 and 28 show the total errors ( $|u_{\text{ex}} - u_{\text{num}}|$ ), as in the case I. The solutions obtained with the schemes developed in [2, 3] are clearly dispersed and dissipated. The solution obtained with the  $SFD_{11}-RK_6(a)$  scheme is also dispersed and dissipated though its total errors are approximately two times lower than the total errors presented by the  $FDo11p-RKB_6$  scheme. In this problem, the solution is only properly calculated by using the new  $SFD_{13}-RK_6(a, b)$  schemes. The solution computed by the  $SFD_{13}-RK_6(a)$  scheme is in phase with the exact one and it results slightly dissipated, whereas the solution computed by the  $SFD_{13}-RK_6(b)$  scheme is the most accurate for this problem.

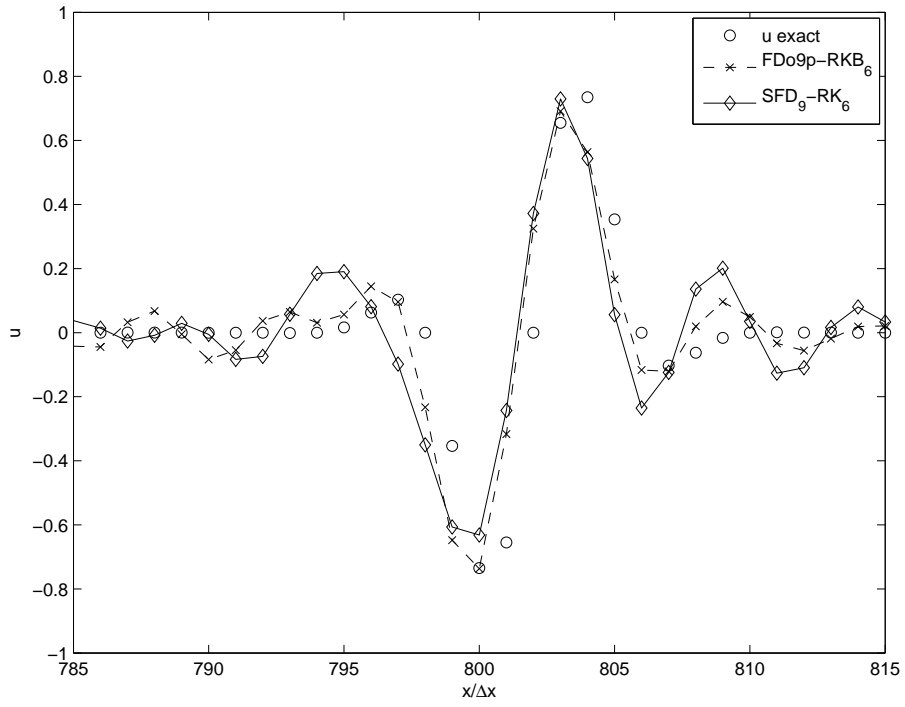


Figure 19: Solution at  $\alpha = 1$  for the schemes  $SFD_9-RK_6(a)$  and  $FDo9p-RKB_6$ .

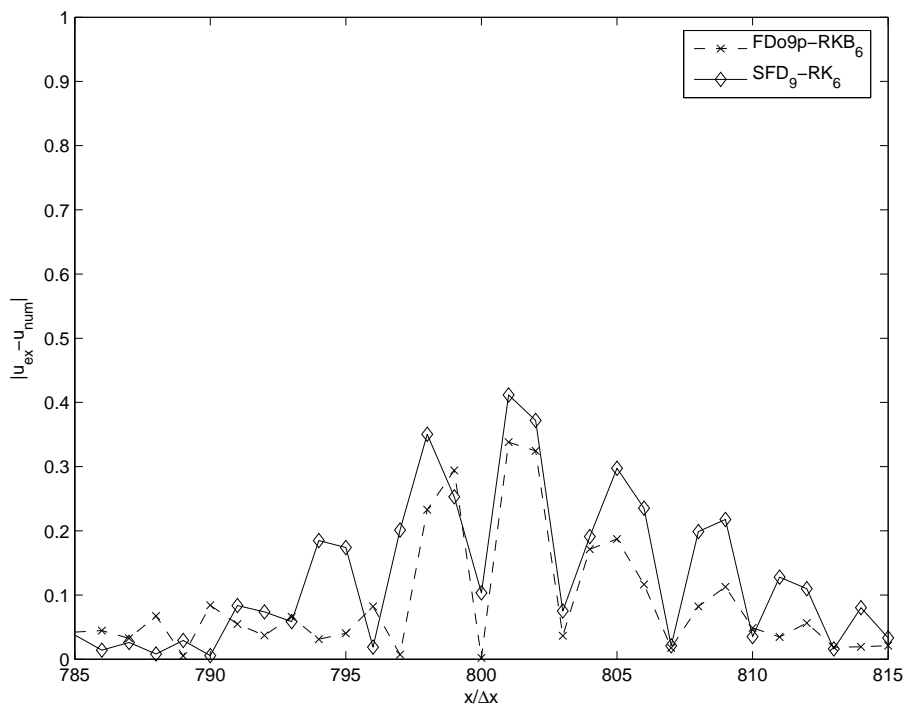


Figure 20: Errors at  $\alpha = 1$  for the schemes  $SFD_9-RK_6(a)$  and  $FDo9p-RKB_6$ .

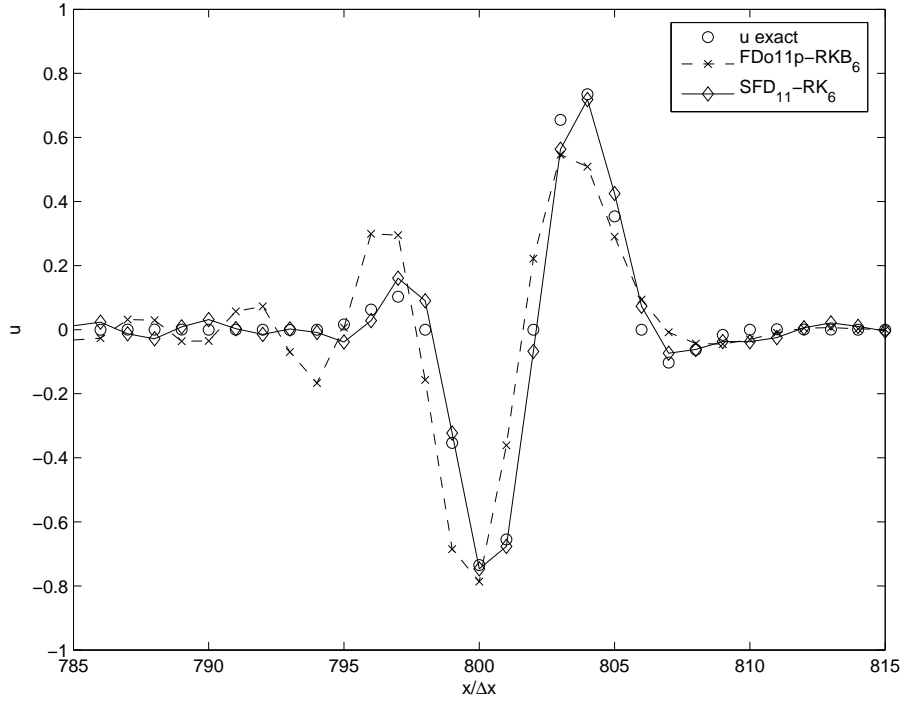


Figure 21: Solution at  $\alpha = 1$  for the schemes  $SFD_{11}-RK_6(a)$  and  $FDo11p-RKB_6$ .

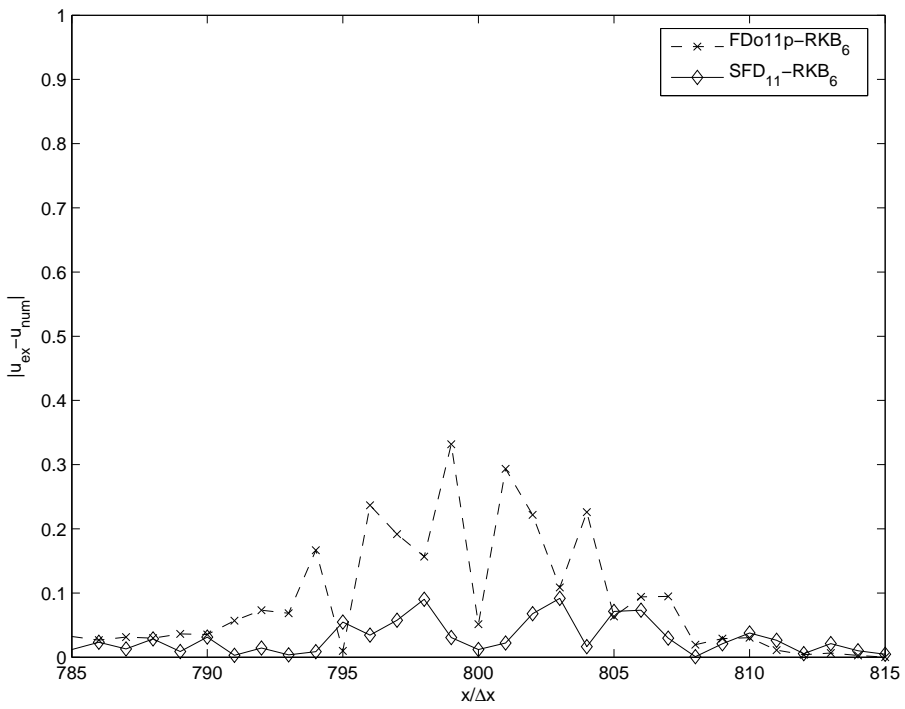


Figure 22: Errors at  $\alpha = 1$  for the schemes  $SFD_{11}-RK_6(a)$  and  $FDo11p-RKB_6$ .

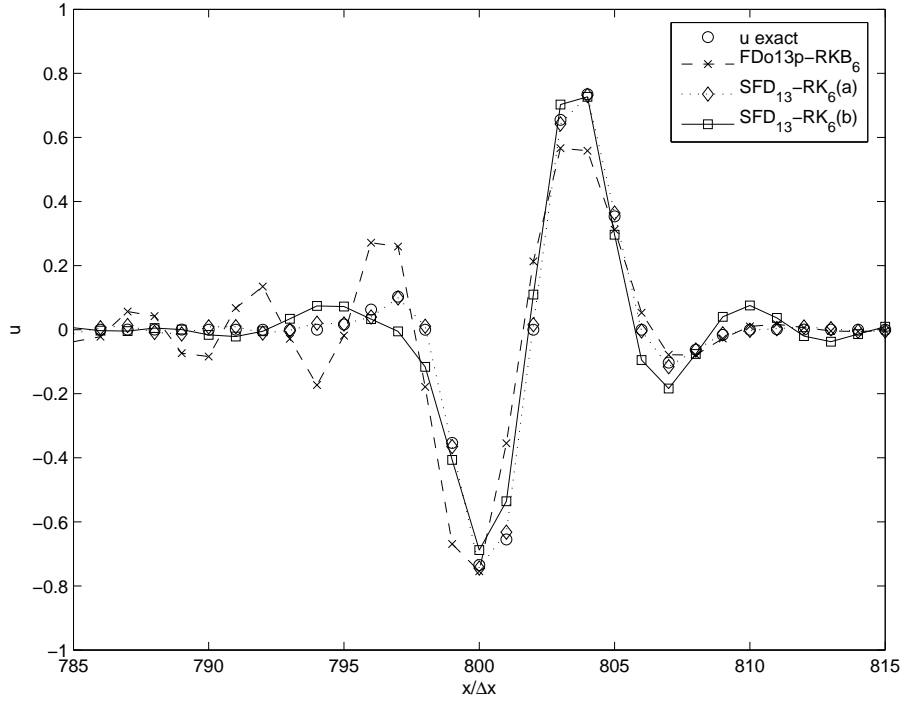


Figure 23: Solution at  $\alpha = 1$  for the schemes  $SFD_{13}\text{-}RK_6(a, b)$  and  $FD013p\text{-}RKB_6$ .

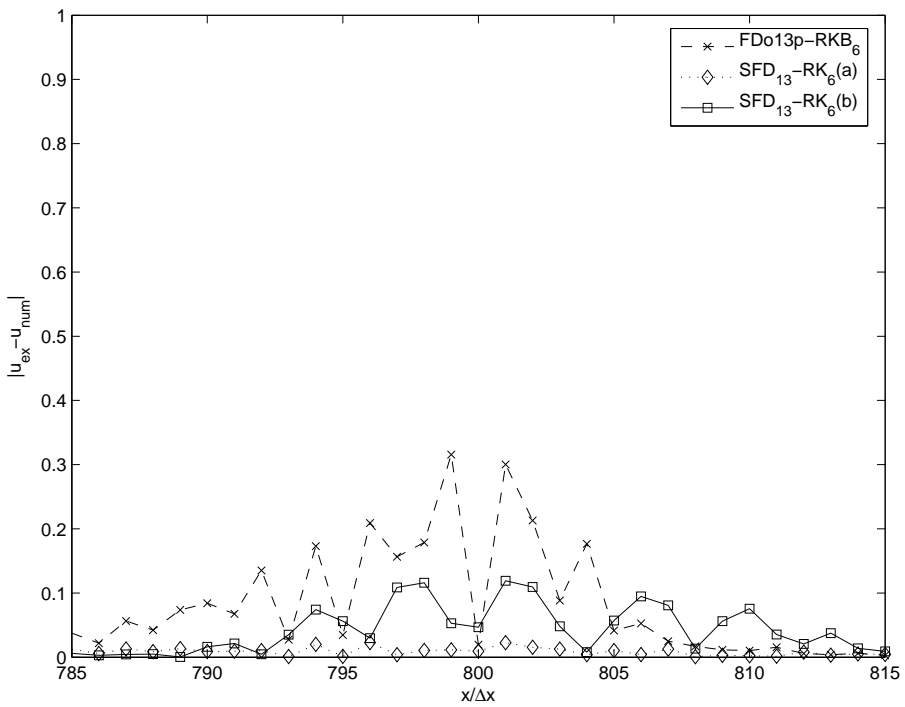


Figure 24: Errors at  $\alpha = 1$  for the schemes  $SFD_{13}\text{-}RK_6(a, b)$  and  $FD013p\text{-}RKB_6$ .

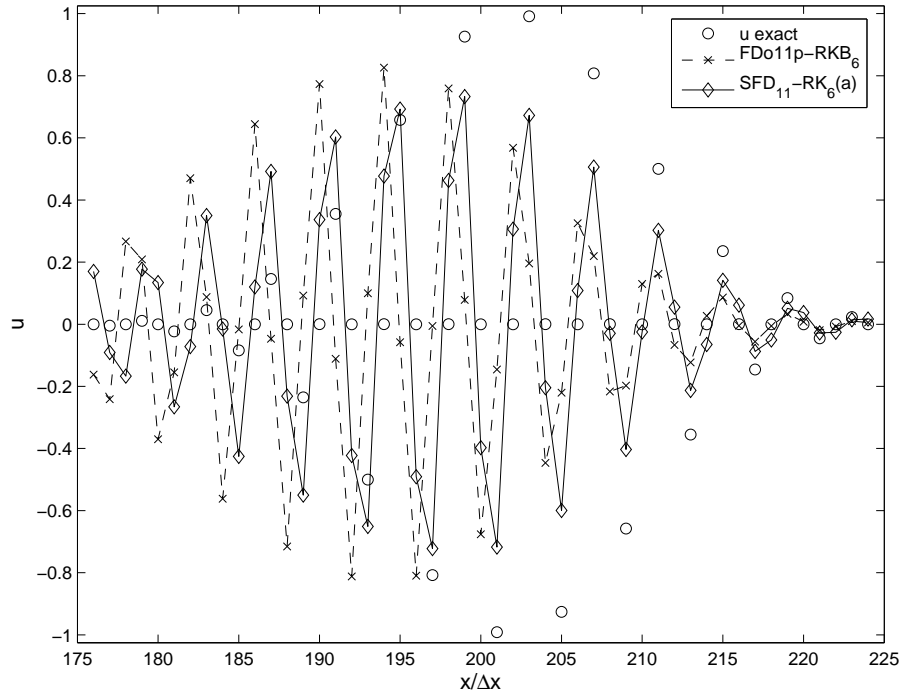


Figure 25: Solution at  $\alpha = 1$  for the schemes  $SFD_{11}-RK_6(a)$  and  $FDo11p-RKB_6$ .

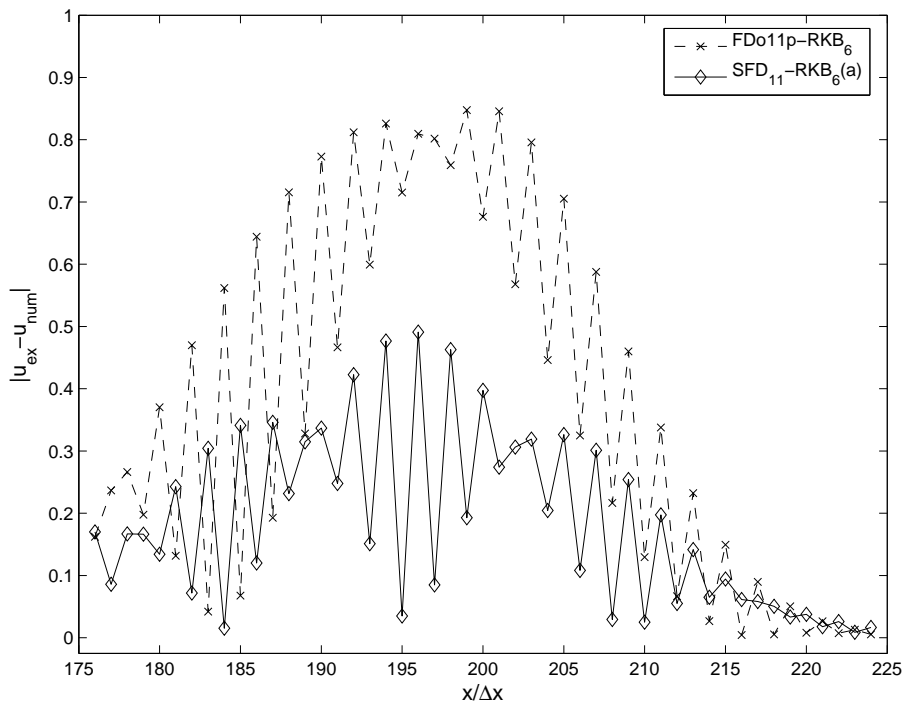


Figure 26: Errors at  $\alpha = 1$  for the schemes  $SFD_{11}-RK_6(a)$  and  $FDo11p-RKB_6$ .

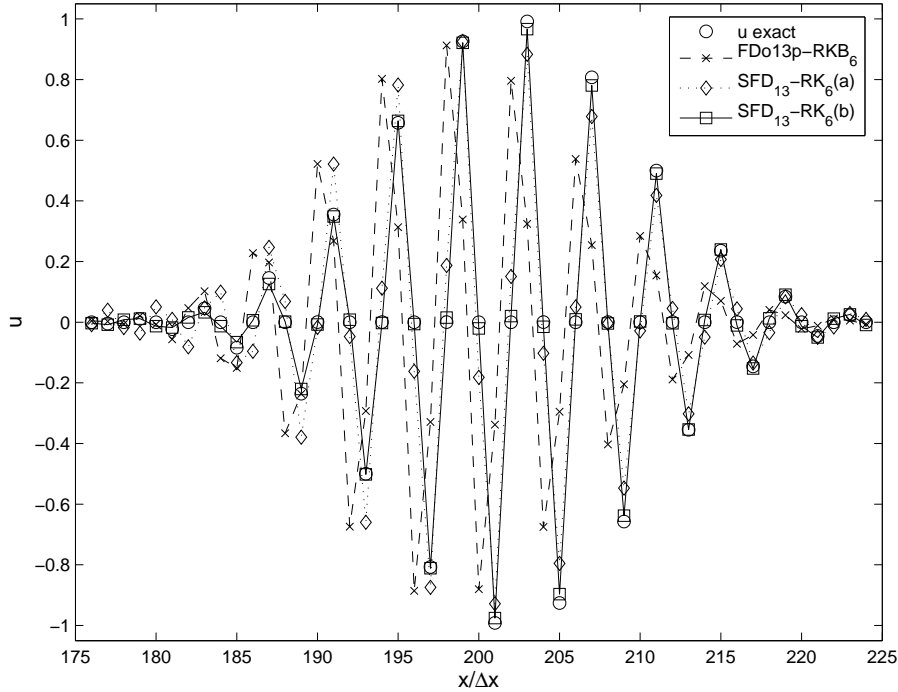


Figure 27: Solution at  $\alpha = 1$  for the schemes  $SFD_{13}\text{-}RK_6(a,b)$  and  $FDo13p\text{-}RKB_6$ .

## 5.2 One dimensional Euler model problems

In our second test problem we consider the one-dimensional linearized Euler equations (around  $u_0, \rho_0, p_0$ )

$$\begin{pmatrix} \rho_t \\ u_t \\ p_t \end{pmatrix} + \begin{pmatrix} u_0 & \rho_0 & 0 \\ 0 & u_0 & \frac{1}{\rho_0} \\ 0 & \gamma p_0 & u_0 \end{pmatrix} \begin{pmatrix} \rho_x \\ u_x \\ p_x \end{pmatrix} = 0. \quad (48)$$

Here  $\rho$  is the density,  $u$  the velocity and  $p$  the pressure. Using the transformation  $(\rho, u, p) \rightarrow (r, v, w)$  given by

$$\rho = \frac{r+w}{c^2} + v, \quad u = \frac{w-r}{c\rho_0}, \quad p = r+w, \quad (49)$$

the PDE system (48) can be written in the diagonal form

$$\begin{pmatrix} r_t \\ v_t \\ w_t \end{pmatrix} + \begin{pmatrix} u_0 - c & 0 & 0 \\ 0 & u_0 & 0 \\ 0 & 0 & u_0 + c \end{pmatrix} \begin{pmatrix} r_x \\ v_x \\ w_x \end{pmatrix} = 0, \quad (50)$$

where  $c = \sqrt{\frac{\gamma p_0}{\rho_0}}$  is the speed of sound, and therefore exact solutions can easily be computed for numerical comparison. We consider the case of subsonic regime,  $0 < u_0 < c$ , for the computations carried out with the FD-RK schemes. The computation domain is

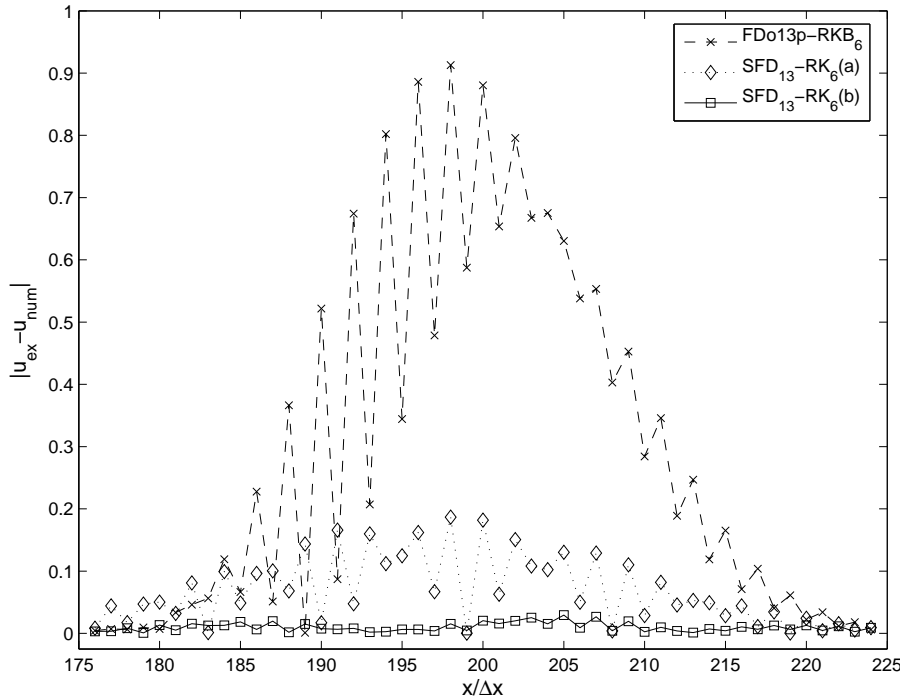


Figure 28: Errors at  $\alpha = 1$  for the schemes  $SFD_{13}\text{-}RK_6(a, b)$  and  $FDo13p\text{-}RKB_6$ .

taken large enough,  $-250 \leq x \leq 250$ , so that boundary conditions do not need to be implemented. The system (48) is solved with  $\Delta x = 1$ ,  $\alpha = 1$ , and the time step size is determined from the CFL number as  $\Delta t = \alpha \Delta x / (u_0 + c)$ . The values of the coefficients are given by  $u_0 = c/10$ ,  $\gamma = 1.4$ ,  $p_0 = 1$ ,  $\rho_0 = 1$ , and the initial perturbation used is

$$\begin{cases} \rho(x, 0) = 1 \\ u(x, 0) = 0 \\ p(x, 0) = e^{-(x/4)^2} \sin(2\pi x/5) \end{cases} \quad (51)$$

The results shown below are obtained after 200 time steps so that  $t_{\text{end}} = 200\Delta t = 153.66$ . Figures 29 and 31 show the density and Figures 30 and 32 show the errors on the density corresponding to the right travelling acoustic wave (it travels at a speed of  $u_0 + c$ ) for the schemes of 11 and 13 points. Here the 9-points schemes do not give accurate solutions in this time interval. As it can be observed in these figures, the  $FDo11p\text{-}RKB_6$  and  $FDo13p\text{-}RKB_6$  schemes present important oscillations behind the acoustic wave. This is due to their total dispersion errors (see Figures 15 and 17). In general, the new optimized schemes show a better dispersive and dissipative behavior than the schemes proposed in [2, 3]. In addition, the errors of the acoustic wave for the new optimizations are smaller in amplitude than those of the schemes proposed in [2, 3]. In particular, the schemes of 13 points present lower trailing oscillations behind the acoustic wave than the schemes of 11 points. In addition, the most accurate results for this problem are given by

the  $SFD_{13}\text{-}RK_6(b)$  scheme.

Finally we consider a nonlinear test problem, the one-dimensional Euler equations

$$\begin{pmatrix} \rho_t \\ u_t \\ p_t \end{pmatrix} + \begin{pmatrix} u & \rho & 0 \\ 0 & u & \frac{1}{\rho} \\ 0 & \gamma p & u \end{pmatrix} \begin{pmatrix} \rho_x \\ u_x \\ p_x \end{pmatrix} = 0. \quad (52)$$

The initial perturbation used is a Gaussian pressure pulse at the center of the domain given by

$$\begin{cases} \rho(x, 0) = 1 \\ u(x, 0) = 0 \\ p(x, 0) = \frac{1}{\gamma} + \Delta p e^{-\beta x^2} \end{cases} \quad (53)$$

where  $\gamma = 1.4$ ,  $\beta = 0.05$  and  $\Delta p = 0.035$ . The computation domain is taken large enough,  $-400 \leq x \leq 400$ , so that boundary conditions do not need to be implemented. The system (52) is solved in dimensionless form with  $\alpha = 1$ ,  $c = 1$ , and the time step is determined from the CFL number as  $c \Delta t = \alpha \Delta x$ . The time integration is propagated up to  $t_{\text{end}} = 150$  for several values of the grid-size  $\Delta x$ . For numerical comparison we have computed a reference solution by using thirtieth-order thirty-one-point standard finite differences for spatial derivation and the six-stage RK algorithm  $RKB_6$  with the CFL number  $\alpha = 0.01$  for time integration as in [2]. The initial perturbation and the computed reference solution for the pressure are shown in Figures 33 and 34, respectively. The error is evaluated as

$$\text{error} = \sum_{i=1}^N |p_{\text{ref}}(x_i) - p_{\text{num}}(x_i)|, \quad (54)$$

where  $N$  is the number of mesh points and  $p_{\text{ref}}$  the reference solution.

Figures 35 and 36 show the errors as a function of the grid-size  $\Delta x$  (in logarithmic scale) for the schemes of 9, 11 and 13 points. As it can be observed, for a grid-size  $\Delta x$  lower than 0.5, the order of accuracy defines the slope of the error curve. In this case all the schemes considered here present accuracy of fourth-order. On the other hand, when  $\Delta x$  is greater than 0.5, the slope of the error curve appears influenced by the dispersion and dissipation errors. Finally, we have observed that for this problem the most accurate results are given by the schemes  $SFD_{13}\text{-}RK_6(a)$  and  $FDo11p\text{-}RKB_6$ .

## 6 Conclusions

A class of optimized explicit methods constituted by symmetric FD schemes for spatial derivation and low storage RK algorithms for time integration is proposed. The methods

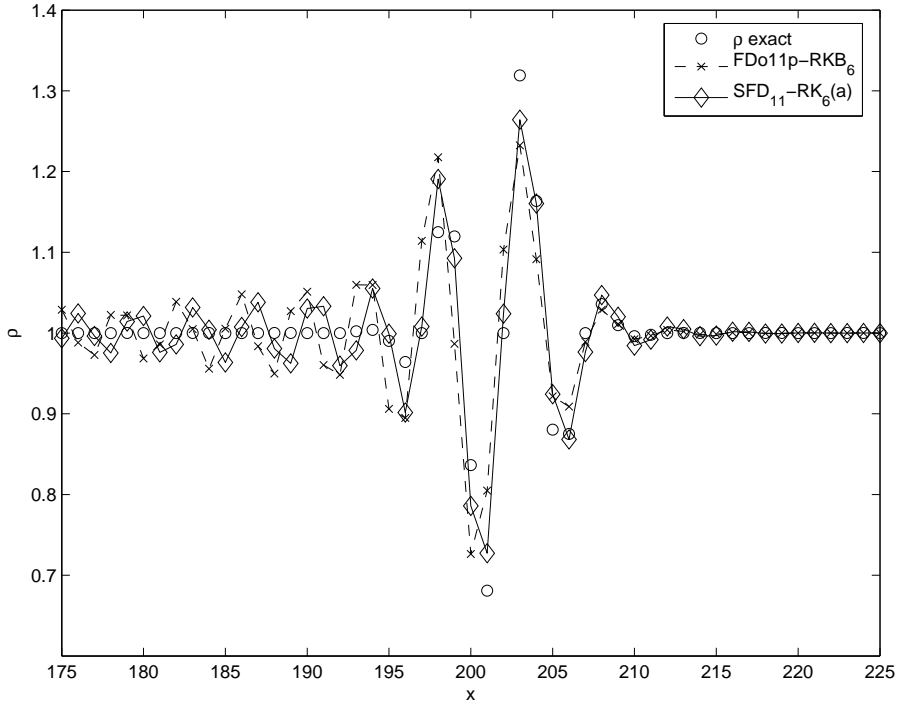


Figure 29: Density for the schemes  $SFD_{11}-RK_6(a)$  and  $FD011p-RKB_6$ .

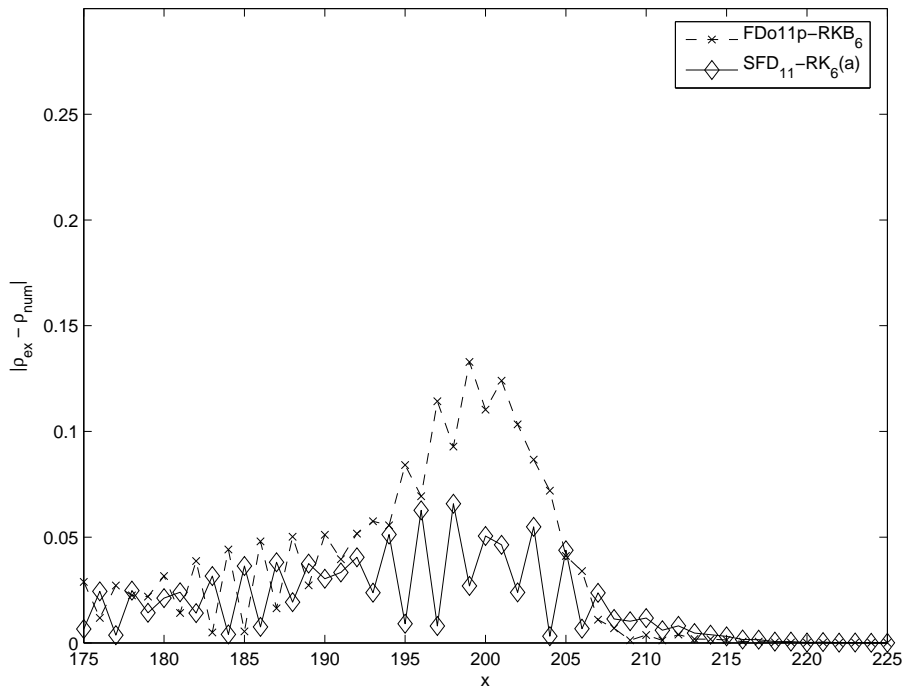


Figure 30: Errors on the density for the schemes  $SFD_{11}-RK_6(a)$  and  $FD011p-RKB_6$ .

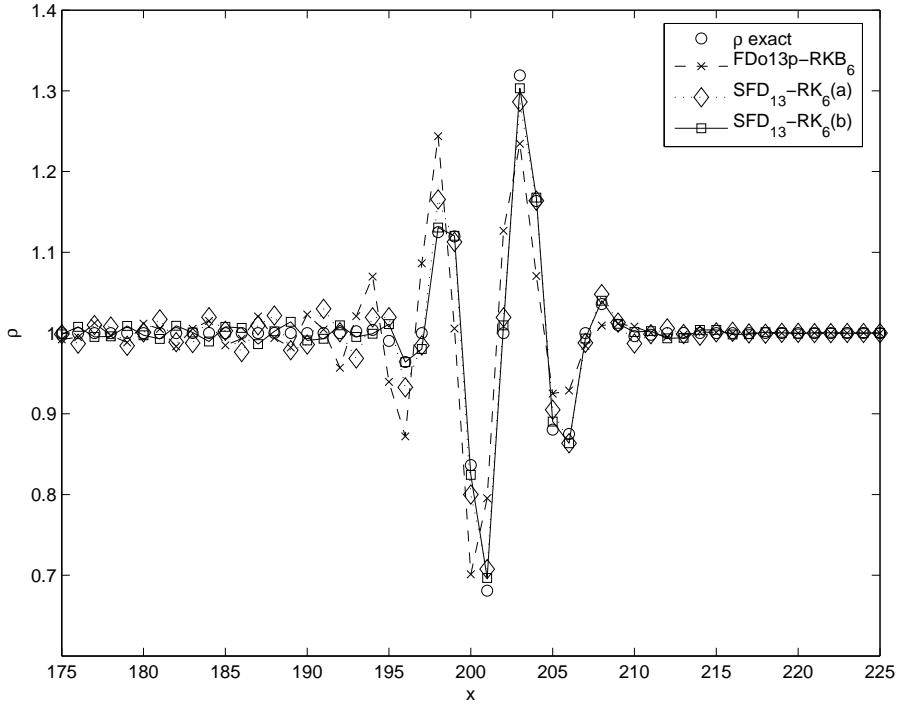


Figure 31: Density for the schemes  $SFD_{13-RK_6}(a,b)$  and  $FDo13p-RKB_6$ .

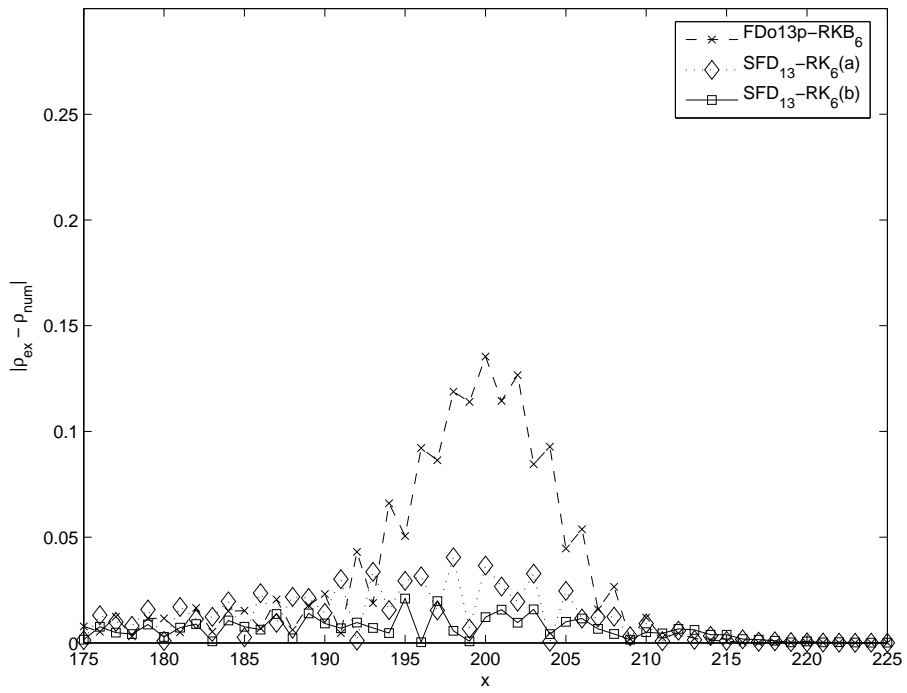


Figure 32: Errors on the density for the schemes  $SFD_{13-RK_6}(a,b)$  and  $FDo13p-RKB_6$ .

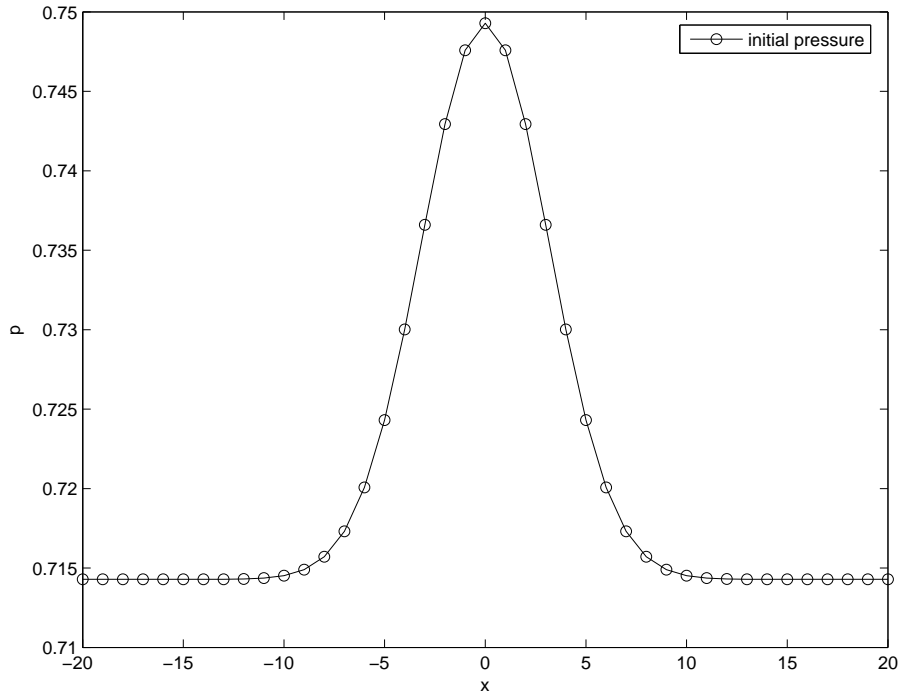


Figure 33: Initial pressure for the 1D Euler equations.

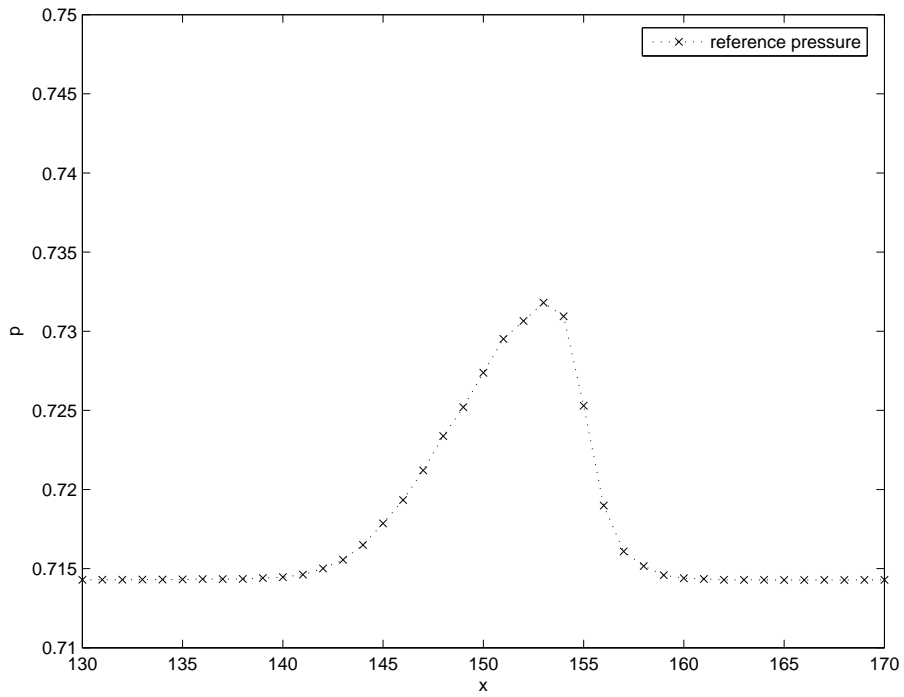


Figure 34: Reference pressure computed at  $t = 150$  for the 1D Euler equations.

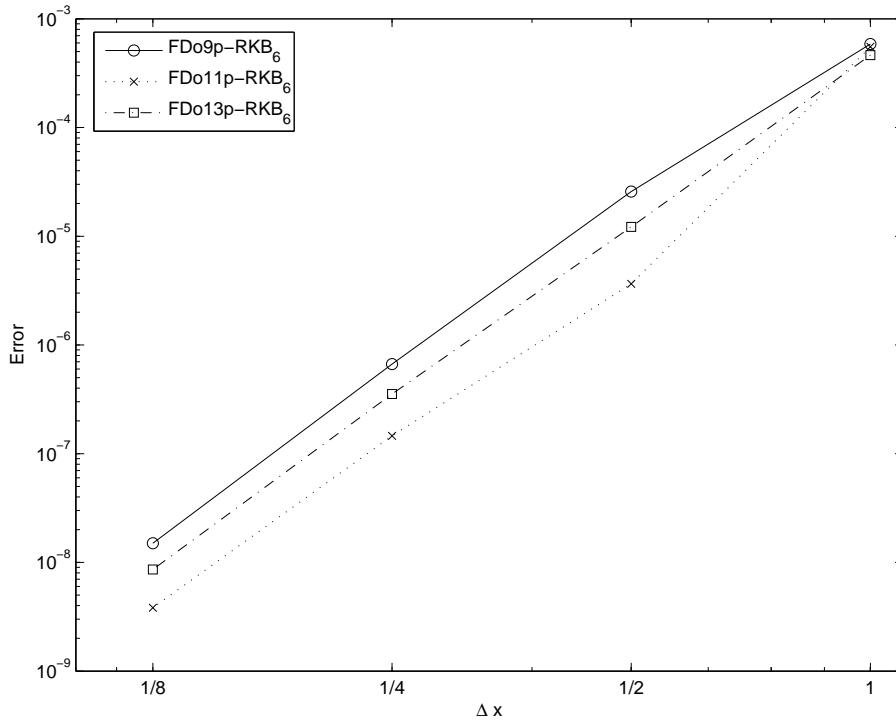


Figure 35: Propagation error as a function of  $\Delta x$  for the schemes of [2, 3].

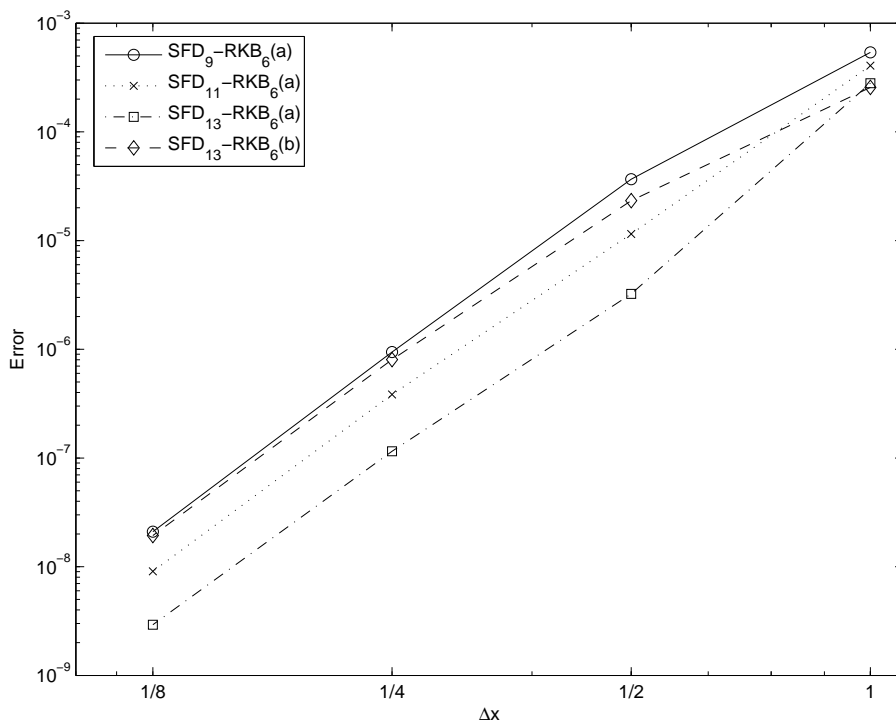


Figure 36: Propagation error as a function of  $\Delta x$  for the new schemes.

are characterized by the minimization of an error measure which takes into account the total dispersion and dissipation errors associated to spatial and temporal discretizations. This new approach allows to optimize the spatial scheme and the time advancement method simultaneously, in opposition to approaches followed by other authors. Optimizations were done on fourth-order symmetric FD schemes with 9, 11 and 13 points in combination with six-stage fourth-order explicit RK algorithms. Analysis of total dispersion and dissipation errors and evaluation of accuracy limits demonstrate the better dispersive properties of the new optimized methods when they are compared with the optimized schemes of [2, 3]. The numerical experiments carried out with 1D convection equations and 1D Euler model problems confirm the improvements in accuracy and efficiency of the new optimizations.

## 7 Future work

In the case of explicit RK methods we will investigate low-storage schemes when they are applied to solve differential problems related with the property of Total Variation Diminishing (TVD). When a RK method is used to solve an IVP:

$$U'(t) = F(U(t)), \quad U(t_0) = U_0 \quad (55)$$

resulting from an application of the method of lines to a Cauchy problem for a PDE, it yields approximations  $U_n = (U_{n,1}, \dots, U_{n,N})^T$  to the exact solution  $U(n\Delta t)$  at  $t_n = n\Delta t$ , where  $\Delta t > 0$  denotes the temporal step-size.

The property of TVD is

$$\|U_{n+1}\|_{TV} \leq \|U_n\|_{TV} \quad (56)$$

where  $\|\cdot\|_{TV}$  is the seminorm defined by

$$\|U_n\|_{TV} = \sum_j |U_{n,j+1} - U_{n,j}|. \quad (57)$$

The main goal is the construction of high-order TVD Runge–Kutta schemes with the property of low-storage while preserving the TVD property.

Other research related with low-storage Runge–Kutta schemes is the analysis and study of new embedded pairs. It is well known that using a fixed step size policy is usually less efficient than allowing the step size to vary each step. Modern explicit Runge–Kutta methods have an error estimator that makes it possible to determine suitable step sizes to adjust dynamically the length of the step size in terms of the behavior of the local solution.

## References

- [1] V. Allampalli, R. Hixon, M. Nallasamy and S.D. Sawyer. High-accuracy large-step explicit Runge–Kutta (HALE-RK) schemes for computational aeroacoustics, *J. Comput. Phys.* **228**, 3837–3850 (2009).
- [2] J. Berland, C. Bogey, C. Bailly: Optimized explicit schemes: matching and boundary schemes and 4th-order Runge–Kutta algorithm, 10th AIAA/CEAS Aeroacoustics Conference, Paper AIAA 2004-2814.
- [3] C. Bogey, C. Bailly: A family of low dispersive and low dissipative explicit schemes for flow and noise computations, *J. Comput. Phys.*, **194** (2004) 194–214.
- [4] M. Calvo, J.M. Franco, L. Rández: Minimum storage Runge–Kutta schemes for computational acoustics, *Comp. Math. Appl.*, **45** (2003) 535–545.
- [5] M. Calvo, J.M. Franco, L. Rández: A new minimum storage Runge–Kutta scheme for computational acoustics, *J. Comput. Phys.*, **201** (2004) 1–12.
- [6] M. Calvo, J.M. Franco, L. Rández: Highly stable RK time advancing schemes for Computational Aero Acoustics, *Bol. Soc. Esp. Mat. Apl.* **50**, (2010), 83–99.
- [7] M. Calvo, J.M. Franco, L. Rández: On some new low storage implementations of time advancing Runge–Kutta methods, *J. Computational Applied Mathematics*, Vol. 236, **15** (2012), 3665–3675.
- [8] M.H. Carpenter, C.A. Kennedy: A fourth-order  $2N$ -storage Runge–Kutta scheme, NASA TR TM109112, June 1994.
- [9] E. Hairer, S.P. Norsett, G. Wanner: *Solving Ordinary Differential Equations I: Non-stiff Problems*, Springer–Verlag, Berlin, 1993.
- [10] Z. Haras, S. Ta’asan: Finite difference schemes for long-time integration, *J. Comput. Phys.*, **114** (1994) 265–279.
- [11] P. J. van der Houwen: *Construction of Integration Formulas for Initial Value Problems*, North-Holland, Amsterdam (1977).
- [12] F.Q. Hu, M.Y. Hussaini, J. Manthey: Low-dissipation and low-dispersion Runge–Kutta schemes for computational acoustics, *J. Comput. Phys.*, **124** (1996) 177–191.
- [13] C.A. Kennedy, M.H. Carpenter, R.M. Lewis: Low-storage, explicit Runge–Kutta schemes for the compressible Navier–Stokes equations, NASA/CR-1999-209349, ICASE Report No. 99-22, 1999.

- [14] D. I. Ketcheson, Highly efficient strong stability preserving Runge–Kutta methods with low storage implementations, *SIAM Journal on Scientific Computing*, **30**, 2113–2136 (2008).
- [15] D. I. Ketcheson, Runge–Kutta Methods with Minimum-Storage Implementations, *Journal of Computational Physics* **229**, 1763–1773 (2010).
- [16] J.W. Kim, D.J. Lee: Optimized compact finite difference schemes with maximum resolution, *AIAA Journal*, **34** (1996) 5.
- [17] S.K. Lele: Compact finite difference schemes with spectral-like resolution, *J. Comput. Phys.*, **103** (1992) 16–42.
- [18] K. Mahesh: A family of high order finite difference schemes with good spectral resolution, *J. Comput. Phys.*, **145** (1998) 332–358.
- [19] J. Ramboer, T. Broeckhoven, S. Smirnov, C. Lacor: Optimization of time integration schemes coupled to spatial discretization for use in CAA applications, *J. Comput. Phys.*, **213** (2006) 777–802.
- [20] D. Stanescu, W.G. Habashi:  $2N$ -storage low dissipation and dispersion Runge–Kutta schemes for computational acoustics, *J. Comput. Phys.*, **143** (1998) 674–681.
- [21] C.K.W. Tam: Computational aeroacoustics: issues and methods, *AIAA Journal*, **33**(10) (1995) 1788–1797.
- [22] C.K.W. Tam, J.C. Webb: Dispersion-relation-preserving finite difference schemes for computational acoustics, *J. Comput. Phys.*, **107** (1993) 262–281.
- [23] J.H. Williamson: Low-storage Runge–Kutta schemes, *J. Comput. Phys.*, **35** (1980) 48–56.

